

Supporting Information for

Evaluation of a Reducible Disulfide Linker for Siderophore-mediated Delivery of Antibiotics

Wilma Neumann and Elizabeth M. Nolan*

Department of Chemistry, Massachusetts Institute of Technology, Cambridge, MA 02139, United States

*Corresponding author: lnolan@mit.edu

Phone: 617-452-2495

This Supporting Information includes:

Methods.....	S5
General Synthetic Materials and Methods	S5
Compounds.....	S6
Reduction of Ent-SS-Cipro 2 by DTT	S7
Enzymatic Siderophore Hydrolysis.....	S7
General Microbiology Materials and Methods	S7
Bacterial Strains	S8
Antimicrobial Activity Assays	S9
Methods References	S9
Supporting Tables.....	S10
Table S1 Bacterial strains.....	S10
Table S2 HPLC retention times of ciprofloxacin derivatives and products from reductive cleavage.....	S11
Table S3 MIC values of the compounds and ciprofloxacin	S12
Supporting Figures	S13
Scheme S1 Initially attempted synthesis of benzyl-protected Ent-SS-Cipro.....	S13
Scheme S2 Hydrolysis of Ent-SS-Cipro 2 by IroD.....	S13
Scheme S3 Structure of DHBS-Cipro	S13
Fig. S1 Cleavage of Ent-SS-Cipro 2 by GSH at pH 7.4.....	S14
Fig. S2 Cleavage of Ent-SS-Cipro 2 by GSH at pH 9.0.....	S15
Fig. S3 Cleavage of Ent-SS-Cipro 2 by TCEP	S16
Fig. S4 Cleavage of Ent-SS-Cipro 2 by DTT	S17
Fig. S5 Cleavage of Cipro-SSEt 4 by GSH at pH 7.4.....	S18
Fig. S6 Cleavage of Cipro-SSEt 4 by GSH at pH 9.0.....	S19
Fig. S7 Cleavage of Cipro-SSEt 4 by TCEP	S20
Fig. S8 Incubation of Cipro-SMe 5 with GSH at pH 7.4.....	S21
Fig. S9 Incubation of Cipro-SMe 5 with GSH at pH 9.0.....	S22
Fig. S10 Incubation of Cipro-SMe 5 with TCEP	S23
Fig. S11 Incubation of Cipro-SH 8 with GSH	S24
Fig. S12 Incubation of Cipro-SH 8 with TCEP	S25

Fig. S13 Analytical HPLC traces of Ent–SS–Cipro 2 , Cipro–SH 8 and ciprofloxacin.....	S26
Fig. S14 Antibacterial activity of Ent–SS–Cipro 2 and DHBS–SS–Cipro 3 , in comparison with Ent–Cipro 1 and DHBS–Cipro, against uropathogenic and non-pathogenic <i>E. coli</i> strains that express IroD.....	S27
Fig. S15 Antibacterial activity of Ent–SS–Cipro 2 and DHBS–SS–Cipro 3 , in comparison with Ent–Cipro 1 and DHBS–Cipro, against <i>E. coli</i> K-12, wild-type and complemented with <i>iroD</i>	S28
Fig. S16 Antibacterial activity of Ent–SS–Cipro 2 and DHBS–SS–Cipro 3 , in comparison with Ent–Cipro 1 and DHBS–Cipro, against non-pathogenic <i>E. coli</i> strains that do not express IroD	S29
Fig. S17 Antibacterial activity of ferric Ent–SS–Cipro 2 in comparison with ferric Ent–Cipro 1 against <i>E. coli</i> BL21(DE3).....	S30
Fig. S18 Antibacterial activity of ferric Ent–SS–Cipro 2 against <i>E. coli</i> B and JB2 in the absence and presence of Ent	S30
Fig. S19 Hydrolysis of Ent–SS–Cipro 2 by IroD	S31
Fig. S20 Analytical HPLC traces of purified Ent–Cipro 1	S31
Fig. S21 Analytical HPLC traces of purified DHBS–Cipro.....	S32
Fig. S22 Analytical HPLC traces of purified Ent–SS–Cipro 2	S32
Fig. S23 Analytical HPLC traces of purified DHBS–SS–Cipro 3	S32
Fig. S24 Analytical HPLC traces of purified Cipro–SSEt 4	S33
Fig. S25 Analytical HPLC traces of purified Cipro–SMe 5	S33
Fig. S26 Optical absorption spectra of the ciprofloxacin derivatives.....	S34
Fig. S27 Optical absorption spectra of apo and ferric Ent–SS–Cipro 2	S34
Fig. S28 ¹ H NMR of 2	S35
Fig. S29 ¹⁹ F NMR of 2	S36
Fig. S30 ¹ H NMR of 4	S37
Fig. S31 ¹⁹ F NMR of 4	S38
Fig. S32 ¹³ C{ ¹ H} NMR of 4	S39
Fig. S33 ¹ H NMR of 5	S40
Fig. S34 ¹⁹ F NMR of 5	S41
Fig. S35 ¹³ C{ ¹ H} NMR of 5	S42
Fig. S36 ¹ H NMR of 7	S43
Fig. S37 ¹⁹ F NMR of 7	S44
Fig. S38 ¹³ C{ ¹ H} NMR of 7	S45
Fig. S39 ¹ H NMR of 8	S46

Fig. S40 ^{19}F NMR of 8	S47
Fig. S41 $^{13}\text{C}\{^1\text{H}\}$ NMR of 8	S48
Fig. S42 ^1H NMR of 9	S49
Fig. S43 ^{19}F NMR of 9	S50
Fig. S44 $^{13}\text{C}\{^1\text{H}\}$ NMR of 9	S51
Fig. S45 ^1H NMR of 12	S52
Fig. S46 $^{13}\text{C}\{^1\text{H}\}$ NMR of 12	S53
Fig. S47 ^1H NMR of Bn ₆ Ent–SS–Cipro	S54
Fig. S48 ^{19}F NMR of Bn ₆ Ent–SS–Cipro	S55

Methods

General Synthetic Materials and Methods

Synthetic Reagents. All commercially available reagents were purchased from Sigma-Aldrich, Alfa-Aesar, TCI America, or P3 BioSystems in the highest available purity and used as received. Reactions were performed under an inert nitrogen atmosphere, except deprotection reactions employing TFA. Dimethylformamide (DMF) and dichloromethane were dried in a VAC solvent purification system (Vacuum Atmospheres); anhydrous dimethyl sulfoxide (DMSO) was purchased from Sigma-Aldrich.

TLC. Analytical thin-layer chromatography (TLC) was performed on pre-coated glass plates (silica gel 60 F₂₅₄; EMD), which were analyzed using UV-light (254 nm; 365 nm for Cipro derivatives). Preparative TLC was performed on pre-coated glass plates with concentrating zone (silica gel 60 F₂₅₄, thickness 2 mm; EMD) and analyzed by UV-light.

HPLC. RP-HPLC was performed on an Agilent 1200 series system with a solvent system, A: 0.1% trifluoroacetic acid (TFA) in Milli-Q water (18.2 mΩ·cm), B: 0.1% TFA in HPLC grade CH₃CN. Absorbance was monitored at 220 nm, 280 nm, 316 nm (catecholate absorption), and 365 nm (quinolone absorption) with a multi-wavelength detector. Analytical RP-HPLC was performed using a Cliepus column (C18, 5-μm pore size, 4.6 mm ID x 250 mm; Higgins Analytical) operated at a flow rate of 1 mL min⁻¹ and a gradient 0–100% B in A over 30 min. Semi-preparative RP-HPLC was performed using a Zorbax column (C18, 5-μm pore size, 9.4 mm ID x 250 mm; Agilent) operated at a flow rate of 4 mL min⁻¹ and a gradient as indicated for the respective compounds.

NMR. NMR spectra were recorded on a Varian Inova-500 NMR spectrometer operating at ambient probe temperature (293 K), housed in the MIT Department of Chemistry Instrumentation Facility. ¹H NMR spectra were recorded at 500 MHz, ¹⁹F NMR spectra at 470 MHz, and ¹³C NMR spectra at 125 MHz. The chemical shifts are reported in ppm relative to the residual solvent peak (CDCl₃, 7.26 ppm for ¹H, 77.16 ppm for ¹³C; DMF-d₇, 8.03 ppm for ¹H);

for ^{19}F NMR, the spectra were referenced through the solvent lock (^2H) signal according to the IUPAC recommended secondary referencing method [1]. Multiplicities are reported using the following abbreviations: s, singlet; br s, broad singlet; d, doublet; t, triplet; q, quadruplet; and m, multiplet.

MS. High-resolution mass spectra were recorded on an Agilent 6510 TOF system with an Agilent Jetstream ESI source, housed at the MIT Center for Environmental Health Sciences.

Optical absorption spectroscopy. Optical absorption spectra were recorded on a Beckman Coulter DU800 spectrophotometer operated at ambient temperature (1 cm quartz cuvettes; Starna).

Compounds

Ent-Cipro **1** [2], DHBS-Cipro (Scheme S3) [3], $\text{Bn}_6\text{EntCOOH}$ **11** [2], and L-Ent [4] were synthesized according to previously reported procedures.

2-((Tritylthio)ethanol (6). The compound was synthesized according to a previously reported procedure [5]. TrtCl (2.0 g, 7.2 mmol) was dissolved in anhydrous THF (5 mL). Mercaptoethanol (0.5 mL, 6.6 mmol) was added and the solution was refluxed for 6 h. The solvent and volatiles were removed *in vacuo*. The white solid was triturated in hexanes/EtOAc 2:1 (30 mL) once, and washed several times with hexanes to yield **6** as white solid (0.8 g, 40%). ^1H NMR (CDCl_3): δ 7.44 (t, $^3J_{\text{H,H}} = 10$ Hz, 6H), 7.30 (t, $^3J_{\text{H,H}} = 10$ Hz, 6H), 7.23 (t, $^3J_{\text{H,H}} = 10$ Hz, 3H), 3.39 (q, $^3J_{\text{H,H}} = 5$ Hz, 2H), 2.50 (t, $^3J_{\text{H,H}} = 5$ Hz, 2H), 1.64 (t, $^3J_{\text{H,H}} = 5$ Hz, 1H). The compound was carried on to the next step without further characterization.

2-(((4-Methoxyphenyl)diphenylmethyl)thio)ethanamine (10). The compound was synthesized according to a previously reported procedure [6]. Cysteamine hydrochloride (0.4 g, 3.4 mmol) was dissolved in TFA (5 mL). MmtCl (1.0 g, 3.2 mmol) was added and the dark red solution was stirred for 4 h under Ar. The TFA was removed *in vacuo*, and the remaining dark orange-red oil was suspended in CH_2Cl_2 . NaOH (3 N) was added and the oil dissolved. The then colorless phases were separated and the organic phase was washed with NaOH (3 N) two more

times. Compound **10** was obtained as colorless oil (1.2 g, 99%). $^1\text{H NMR}$ (CDCl_3): δ 7.43 (d, $^3J_{\text{H,H}} = 8$ Hz, 4H), 7.33 (d, $^3J_{\text{H,H}} = 9$ Hz, 2H), 7.29 (t, $^3J_{\text{H,H}} = 8$ Hz, 5H), 7.21 (t, $^3J_{\text{H,H}} = 7$ Hz, 2H), 6.82 (t, $^3J_{\text{H,H}} = 9$ Hz, 2H), 3.80 (s, 3H), 2.61 (t, $^3J_{\text{H,H}} = 7$ Hz, 2H), 2.33 (t, $^3J_{\text{H,H}} = 7$ Hz, 2H). The compound was carried on to the next step without further characterization.

Reduction of Ent–SS–Cipro 2 by DTT

To a solution containing conjugate **2** (100 μM) in 75 mM Tris-HCl buffer, pH 7.4 or 9.0, DTT (1 mM from a 100 mM stock) was added (final volume: 100 μL). The reaction was incubated at r.t. for 30 min, quenched by adding 6% TFA in Milli-Q water (10 μL), and analyzed by analytical HPLC.

Enzymatic Siderophore Hydrolysis

IroD. The esterase enzyme IroD (N-His₆) was overexpressed in *Escherichia coli* BL21(DE3) and purified by Ni-NTA affinity chromatography as previously reported [7].

Enzymatic hydrolysis of Ent–SS–Cipro 2 with IroD. To a solution containing conjugate **2** (300 μM) in 75 mM Tris-HCl buffer, pH 8.0, IroD (0.3 μM) was added (final volume: 650 μL). The reaction was incubated at r.t., and aliquots (100 μL) were quenched by adding 6% TFA in Milli-Q water (10 μL) at varying time points, and analyzed by analytical HPLC.

General Microbiology Materials and Methods

LB, 5 \times M9 minimal salts, and agar were purchased from BD; casein amino acids were purchased from Amresco. All growth media and Milli-Q water (18.2 $\text{M}\Omega\cdot\text{cm}$, 0.22- μm filter) used for bacterial cultures or for preparing solutions of the tested compounds were sterilized in an autoclave. Sterile polypropylene culture tubes and sterile polystyrene 96-well plates used for culturing were purchased from VWR and Corning Incorporated, respectively.

Growth of *E. coli* under low-Fe conditions was performed employing a modified M9 minimal medium (6.8 g L^{-1} Na_2HPO_4 , 3 g L^{-1} KH_2PO_4 , 0.5 g L^{-1} NaCl , 1 g L^{-1} NH_4Cl , 0.4%

glucose, 2 mM MgSO₄, 0.1 mM CaCl₂, 0.2% casein amino acids, and 16.5 μg mL⁻¹ thiamine) [8]. *E. coli* UTI89 required further supplementation of modified M9 minimal medium with nicotinic acid (0.0025% w/v) due to a mutation in the *nadB* gene encoding L-aspartate oxidase [9]. The iron content of the modified M9 minimal medium was determined by ICP-MS to be 0.6 μM.

Bacterial growth was monitored by recording the optical density at 600 nm (OD₆₀₀) on a Beckman Coulter DU800 spectrophotometer or by using a BioTek Synergy HT plate reader.

Stock solutions of Ent and conjugates **1**, **2** and **3** were prepared in DMSO; stock solutions of compounds **4** and **5** were prepared in DMF (due to insolubility in DMSO); all stocks were aliquoted and stored at -20 °C. The concentration of the stock solutions (ranging from 1 to 25 mM) was determined by dilution with Milli-Q water and measuring the quinolone absorbance at 279 nm (ϵ : 12600 M⁻¹ cm⁻¹, Cipro conjugates). For the Ent stock solution, an aliquot was diluted with MeOH and the catecholate absorbance at 316 nm was measured (ϵ : 9500 M⁻¹ cm⁻¹) [10]. The stock solution of ciprofloxacin (10 mM) was prepared in acidified H₂O (15 μL 12 M HCl in 5 mL H₂O). For antimicrobial assays with conjugates **1**, **2**, **3**, and DHBS-Cipro, working dilutions of the stock solutions and ciprofloxacin were prepared in 10% DMSO/H₂O; the final cultures contained 1% v/v DMSO. For antimicrobial assays with compounds **4** and **5**, working dilutions of the stock solutions and ciprofloxacin were prepared in 10% DMF/H₂O; the final cultures contained 1% v/v DMF. Both 1% v/v DMSO and 1% v/v DMF had negligible effects on the growth of *E. coli* under these conditions. For pre-loading of conjugates **1** and **2** with Fe(III), 0.9 equiv of FeCl₃ (20 mM stock: 27 mg FeCl₃·6H₂O in 125 μL 12 M HCl and 5 mL H₂O) was added to the conjugates and the solutions were incubated for 5 min; formation of the ferric complex of **2** was verified by optical absorption spectroscopy (Figure S27).

Bacterial Strains

Information pertaining to all bacterial strains used in this study is listed in Table S1. Freezer stocks of all *E. coli* strains (except K-12) were prepared from single colonies in 25% glycerol/Luria

Broth (LB) medium; freezer stocks of *E. coli* K-12 were prepared from single colonies in 25% glycerol/M9 minimal medium.

Antimicrobial Activity Assays

Assays with *E. coli* K12(DE3) *iroD*⁺ and BL21(DE3) *iroD*⁺. The assays were performed in modified M9 medium as described in the main text, except that the overnight cultures were supplemented with kanamycin (50 µg/mL).

Competition assays with Ent. The assays were performed in modified M9 medium as described in the main text, except that ferric conjugate **2** was mixed with apo Ent in a 1:1 molar ratio during preparation of the working dilutions.

Methods References

1. Harris Robin K, Becker Edwin D, Cabral de Menezes Sonia M, Goodfellow R, Granger P (2001) *Pure Appl Chem* 73:1795-1818
2. Zheng T, Bullock JL, Nolan EM (2012) *J Am Chem Soc* 134:18388-18400
3. Neumann W, Sassone-Corsi M, Raffatellu M, Nolan EM (2018) *J Am Chem Soc* 140:5193-5201
4. Ramirez RJA, Karamanukyan L, Ortiz S, Gutierrez CG (1997) *Tetrahedron Lett* 38:749-752
5. Cooley CB, Trantow BM, Nederberg F, Kiesewetter MK, Hedrick JL, Waymouth RM, Wender PA (2009) *J Am Chem Soc* 131:16401-16403
6. Riddoch RW, Schaffer P, Valliant JF (2006) *Bioconjugate Chem* 17:226-235
7. Lin H, Fischbach MA, Liu DR, Walsh CT (2005) *J Am Chem Soc* 127:11075-11084
8. Chairatana P, Zheng T, Nolan EM (2015) *Chem Sci* 6:4458-4471
9. Li Z, Bouckaert J, Deboeck F, De Greve H, Hernalsteens JP (2012) *Microbiology* 158:736-745
10. Scarrow RC, Ecker DJ, Ng C, Liu S, Raymond KN (1991) *Inorg Chem* 30:900-906

Supporting Tables

Table S1 Bacterial strains employed in this study.

Strain	Source	Characteristics
<i>E. coli</i> K-12	ATCC	Common lab strain, non-pathogenic
<i>E. coli</i> K-12(DE3) <i>iroD</i> ⁺	Prepared from <i>E. coli</i> K-12 ^a	Complemented with pET-28b- <i>iroD</i> plasmid
<i>E. coli</i> B	ATCC	Common lab strain, non-pathogenic
<i>E. coli</i> BL21(DE3)	Invitrogen	Common lab strain for protein expressions, non-pathogenic
<i>E. coli</i> BL21(DE3) <i>iroD</i> ⁺	Prepared from <i>E. coli</i> BL21(DE3)	Complemented with pET-28b- <i>iroD</i> plasmid ^b
<i>E. coli</i> CFT073	ATCC	Clinical isolate, UPEC ^c , expression of IroD
<i>E. coli</i> UTI89	Prof. L. Cegelski (Stanford University)	Clinical isolate, UPEC ^c , expression of IroD
<i>E. coli</i> Nissle 1917	Ardeypharm GmbH (Herdecke, Germany)	Probiotic strain, expression of IroD
<i>E. coli</i> JB2	Prof. M. Raffatellu (UC San Diego)	Mouse gut commensal isolate ^d

^a Neumann W, Sassone-Corsi M, Raffatellu M, Nolan EM (2018) *J Am Chem Soc* 140:5193-5201. ^b Lin H, Fischbach MA, Liu DR, Walsh CT (2005) *J Am Chem Soc* 127:11075-11084.

^c UPEC, uropathogenic *E. coli*. ^d Behnsen J, Jellbauer S, Wong CP, Edwards RA, George MD, Ouyang W, Raffatellu M (2014) *Immunity* 40:262-273.

Table S2 HPLC retention times of ciprofloxacin derivatives and products from reductive cleavage.

Substrate	Product	Retention time (min)
Ent–SS–Cipro (2)	–	21.6
Cipro–SSEt (4)	–	25.2
Cipro–SMe (5)	–	22.5 (18.5) ^a
Cipro–SH (8)	–	22.0
Ciprofloxacin	–	14.0
Ent–SS–Cipro (2) + GSH (Fig. S1, S2)	–	21.6
	Cipro–SH (8)	22.1
	Ent–SH ^b	17.8
	Cipro–SSG ^b	17.6
	Ent–SSG ^b	15.7
	Ciprofloxacin	14.2
Ent–SS–Cipro (2) + TCEP (Fig. S3)	–	21.8
	Cipro–SH (8)	22.1
	Ent–SH ^b	17.8
	Ciprofloxacin	14.2
Cipro–SSEt (4) + GSH (Fig. S5, S6)	–	25.3
	Cipro–SH (8)	22.0
	Cipro–SSG ^b	17.6
	Ciprofloxacin	14.1
Cipro–SSEt (4) + TCEP (Fig. S7)	–	25.3
	Cipro–SH (8)	22.0
	Ciprofloxacin	14.1
Cipro–SMe (5) + GSH (Fig. S8, S9)	–	22.5 (18.5) ^a
	No product	–
Cipro–SMe (5) + TCEP (Fig. S10)	–	22.5 (18.4) ^a
	No product	–
Cipro–SH (8) + GSH (Fig. S11)	–	22.0
	Ciprofloxacin	14.1
Cipro–SH (8) + TCEP (Fig. S12)	–	22.0
	Ciprofloxacin	14.0

^a When dissolved in Tris buffer, compound **5** elutes as two distinct peaks; see Fig. S25 for analytical HPLC traces indicating purity. ^b The identity of the products was assigned based on retention times and absorbance at 316 nm (catecholate absorption) or 365 nm (quinolone absorption), respectively.

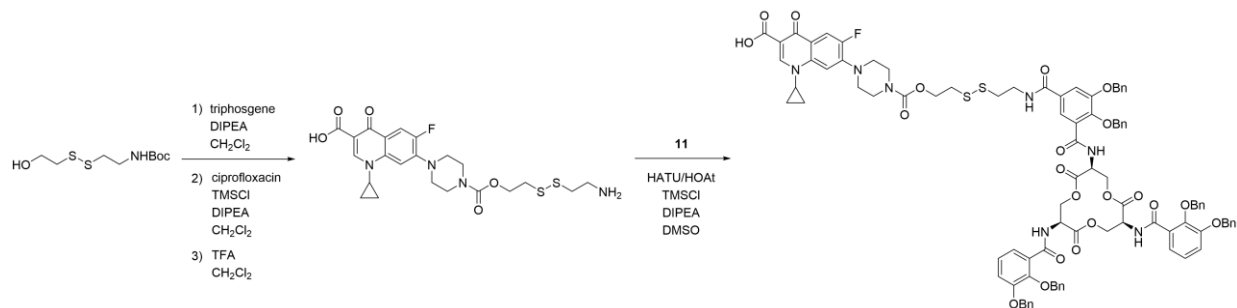
Table S3 MIC values of the compounds and ciprofloxacin for the inhibition of pathogenic and non-pathogenic *E. coli* strains in modified M9 medium. The conjugates **1** and **2** were pre-loaded with 0.9 equiv Fe(III).

	<i>E. coli</i> UTI89		<i>E. coli</i> CFT073		<i>E. coli</i> Nissle 1917	
	μM	$\mu\text{g/mL}$	μM	$\mu\text{g/mL}$	μM	$\mu\text{g/mL}$
1	0.1	0.1	1	1.1	1	1.1
2	>10	>12	>10	>12	10	12
3	>10	>8	>10	>8	>10	>8
4	>10	>5	>10	>5	n.d.	n.d.
5	>10	>5	>10	>5	n.d.	n.d.
Ciprofloxacin	0.1	0.03	0.1	0.03	0.1	0.03

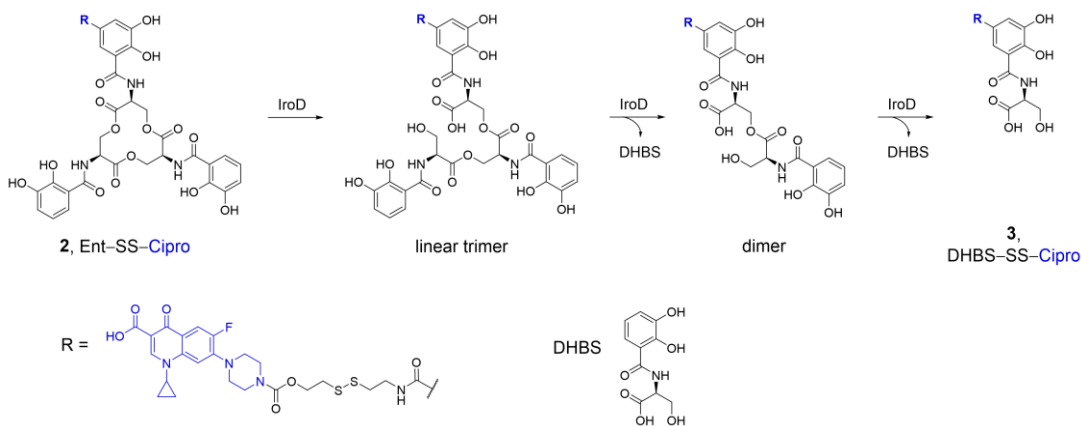
	<i>E. coli</i> K-12		<i>E. coli</i> B		<i>E. coli</i> JB2	
	μM	$\mu\text{g/mL}$	μM	$\mu\text{g/mL}$	μM	$\mu\text{g/mL}$
1	>10	>11	10	11	>10	>11
2	>10	>12	0.1	0.1	1	1.2
3	>10	>8	>10	>8	>10	>8
4	n.d.	n.d.	10	5	>10	>5
5	n.d.	n.d.	10	5	10	5
Ciprofloxacin	0.1	0.03	0.01	0.03	0.1	0.03

n.d., not determined.

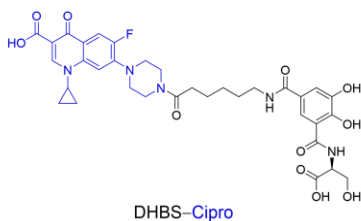
Supporting Figures



Scheme S1 Initially attempted synthesis of benzyl-protected Ent-SS-Cipro.



Scheme S2 Hydrolysis of Ent-SS-Cipro **2** by IroD. The regioselectivity of IroD on Ent-SS-Cipro **2** for formation of the linear trimer and dimer was not determined; only one possible sequence for the hydrolysis of the ester bonds is shown.



Scheme S3 Structure of DHBS-Cipro, which is formed by IroD-catalyzed hydrolysis of Ent-Cipro **1**.

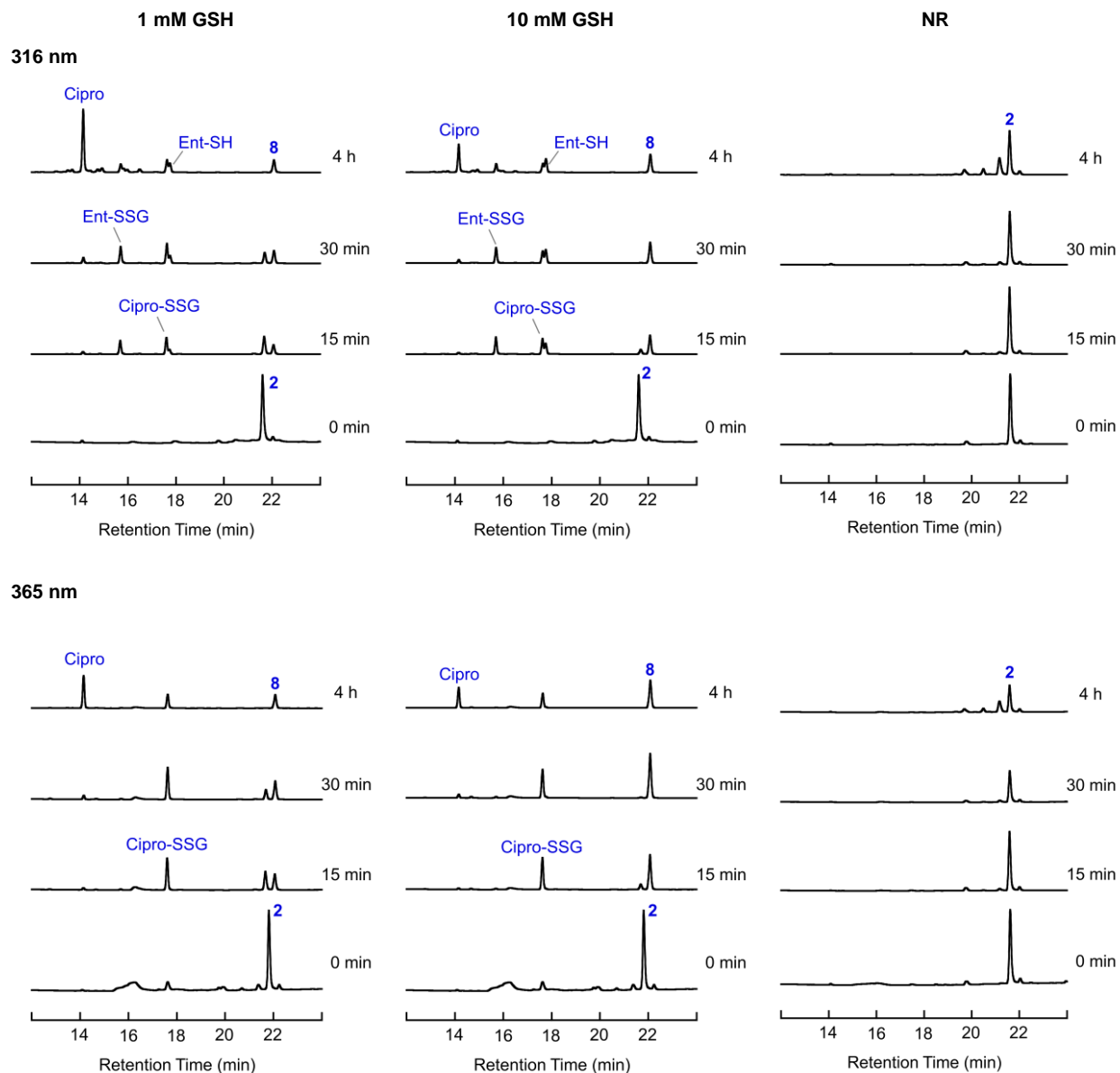


Fig. S1 Cleavage of Ent-SS-Cipro **2** by GSH at pH 7.4. Analytical HPLC traces of 100 μ M Ent-SS-Cipro incubated with 1 or 10 mM GSH in 75 mM Tris-HCl, pH 7.4 for the indicated time; aliquots were quenched with acid. Absorbance monitored at 316 nm (top panel) and 365 nm (bottom panel); NR, no-reductant control. The trace at 316 nm for the incubation with 1 mM GSH corresponds to Fig. 1a and is included for direct comparison.

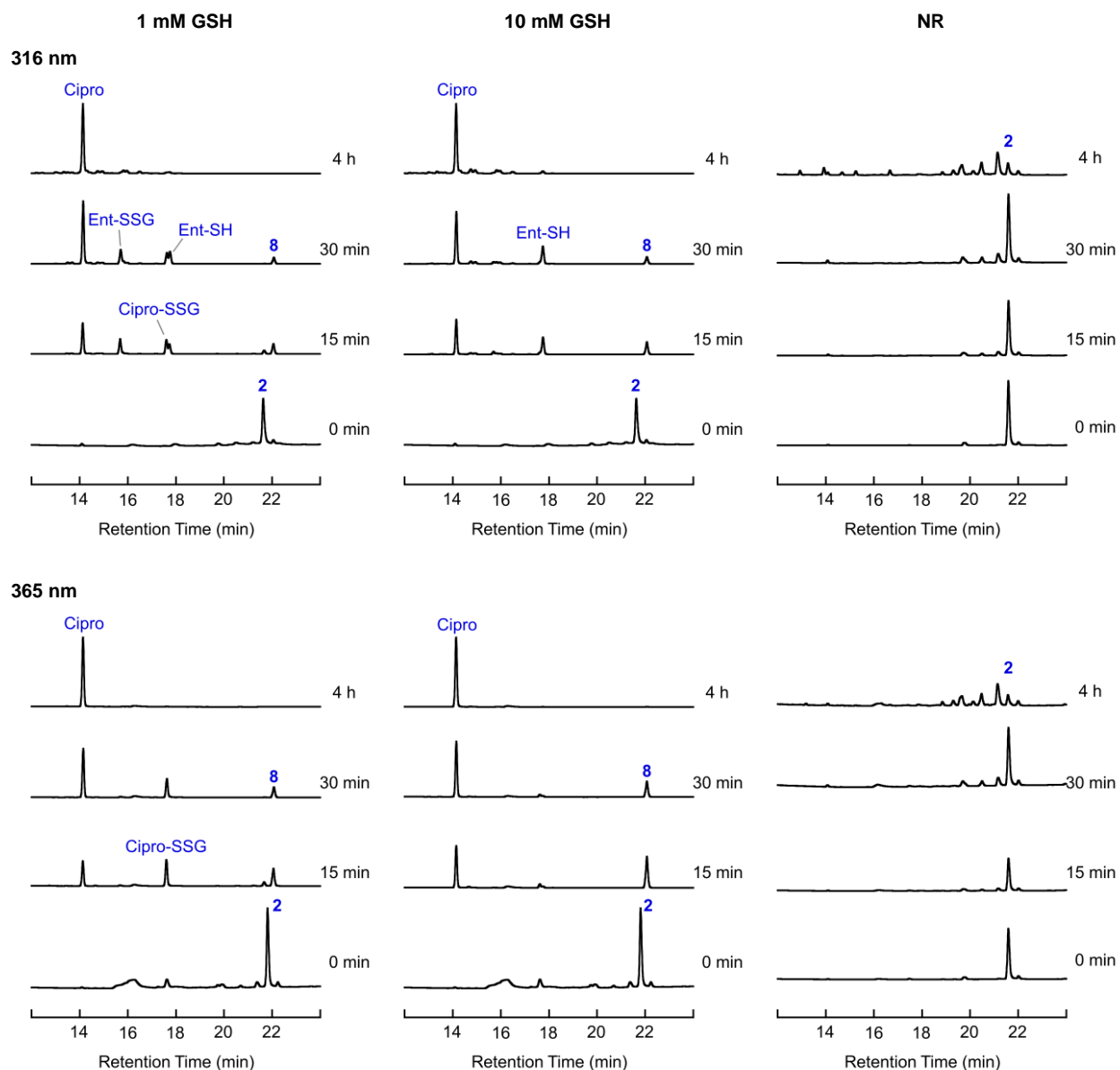


Fig. S2 Cleavage of Ent-SS-Cipro **2** by GSH at pH 9.0. Analytical HPLC traces of 100 μ M Ent-SS-Cipro incubated with 1 or 10 mM GSH in 75 mM Tris-HCl, pH 9.0 for the indicated time; aliquots were quenched with acid. Absorbance monitored at 316 nm (top panel) and 365 nm (bottom panel); NR, no-reductant control. The trace at 316 nm for the incubation with 1 mM GSH corresponds to Fig. 1b and is included for direct comparison.

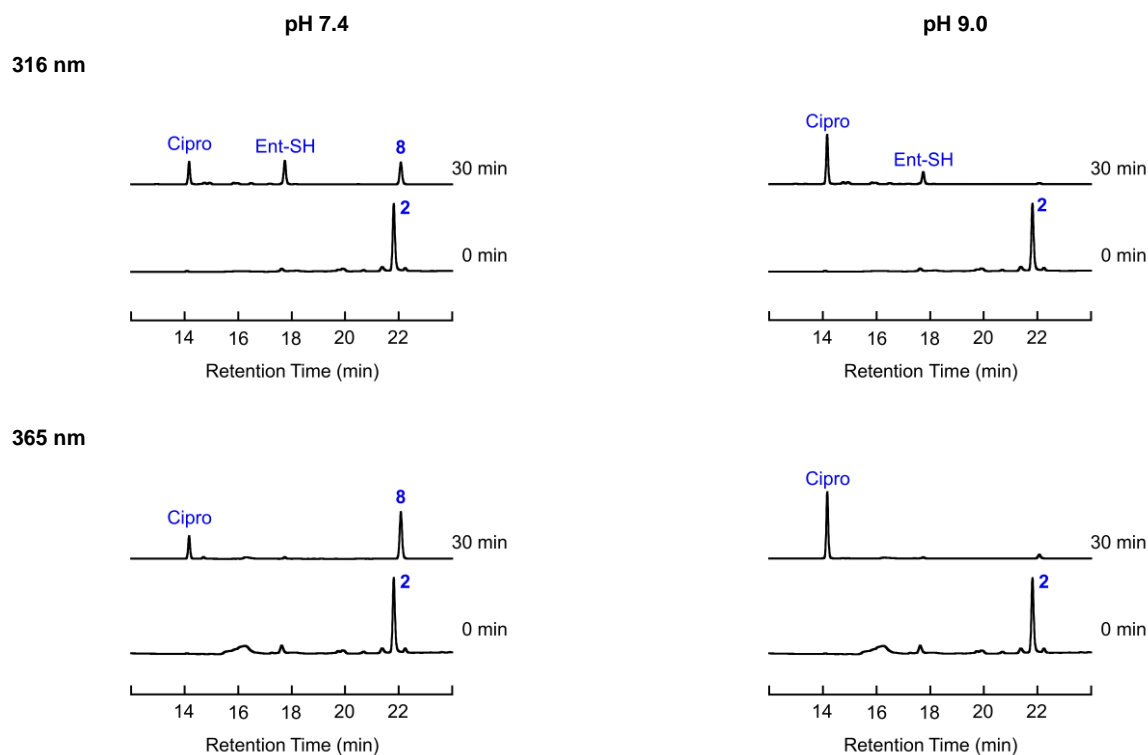


Fig. S3 Cleavage of Ent-SS-Cipro **2** by TCEP at pH 7.4 and pH 9.0. Analytical HPLC traces of 100 μ M Ent-SS-Cipro incubated with 1 mM TCEP in 75 mM Tris-HCl, pH 7.4 or 9.0 for the indicated time; aliquots were quenched with acid. Absorbance monitored at 316 nm (top panel) and 365 nm (bottom panel). The traces at 316 nm for the incubation with 1 mM TCEP correspond to Fig. 1c and 1d, respectively, and are included for direct comparison.

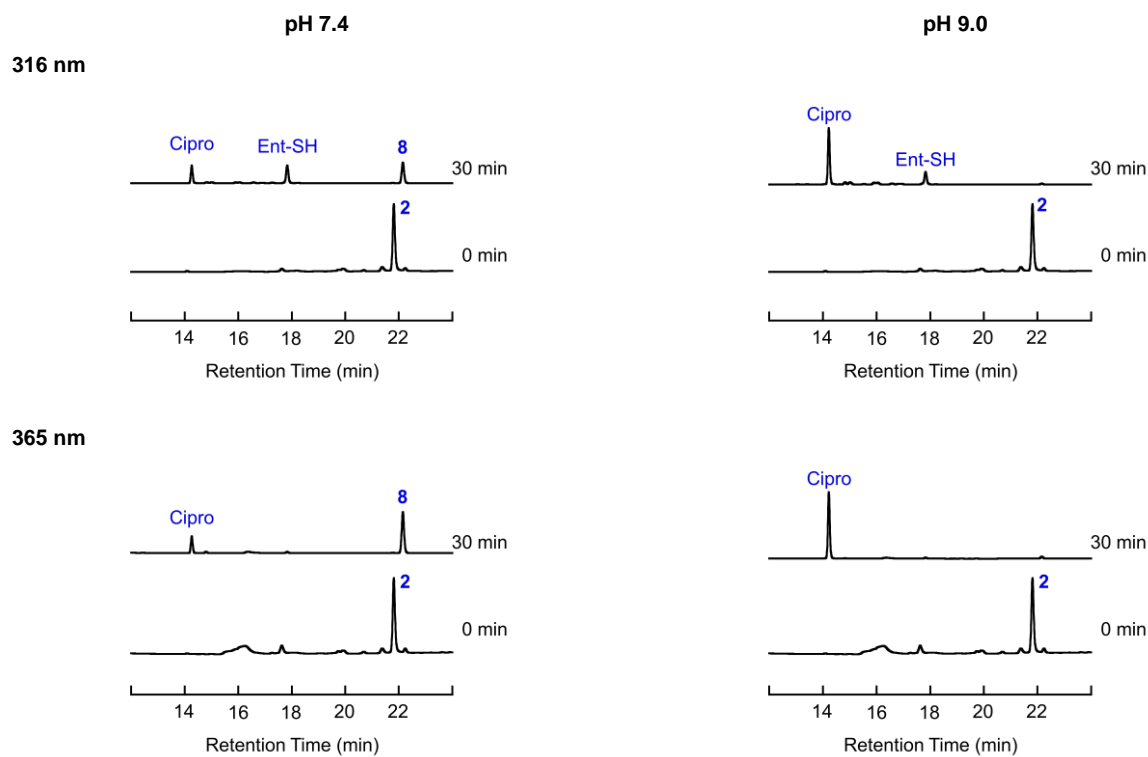


Fig. S4 Cleavage of Ent-SS-Cipro **2** by DTT at pH 7.4 and 9.0. Analytical HPLC traces of 100 μ M Ent-SS-Cipro incubated with 1 mM DTT in 75 mM Tris-HCl, pH 7.4 or 9.0 for the indicated time; aliquots were quenched with acid. Absorbance monitored at 316 nm (top panel) and 365 nm (bottom panel).

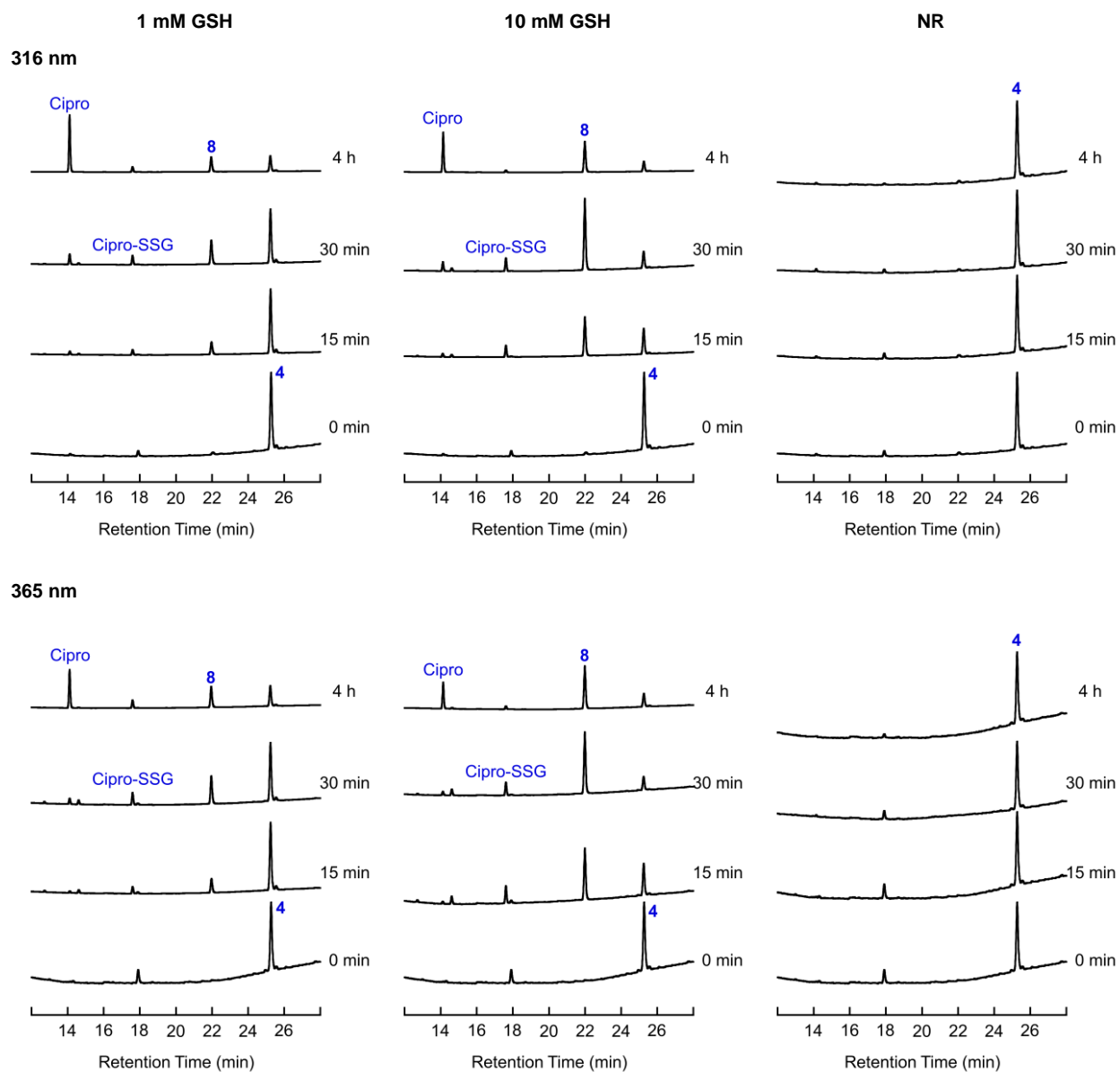


Fig. S5 Cleavage of Cipro–SSEt **4** by GSH at pH 7.4. Analytical HPLC traces of 100 μ M Cipro–SSEt incubated with 1 or 10 mM GSH in 75 mM Tris-HCl, pH 7.4 for the indicated time; aliquots were quenched with acid. Absorbance monitored at 316 nm (top panel) and 365 nm (bottom panel); NR, no-reductant control.

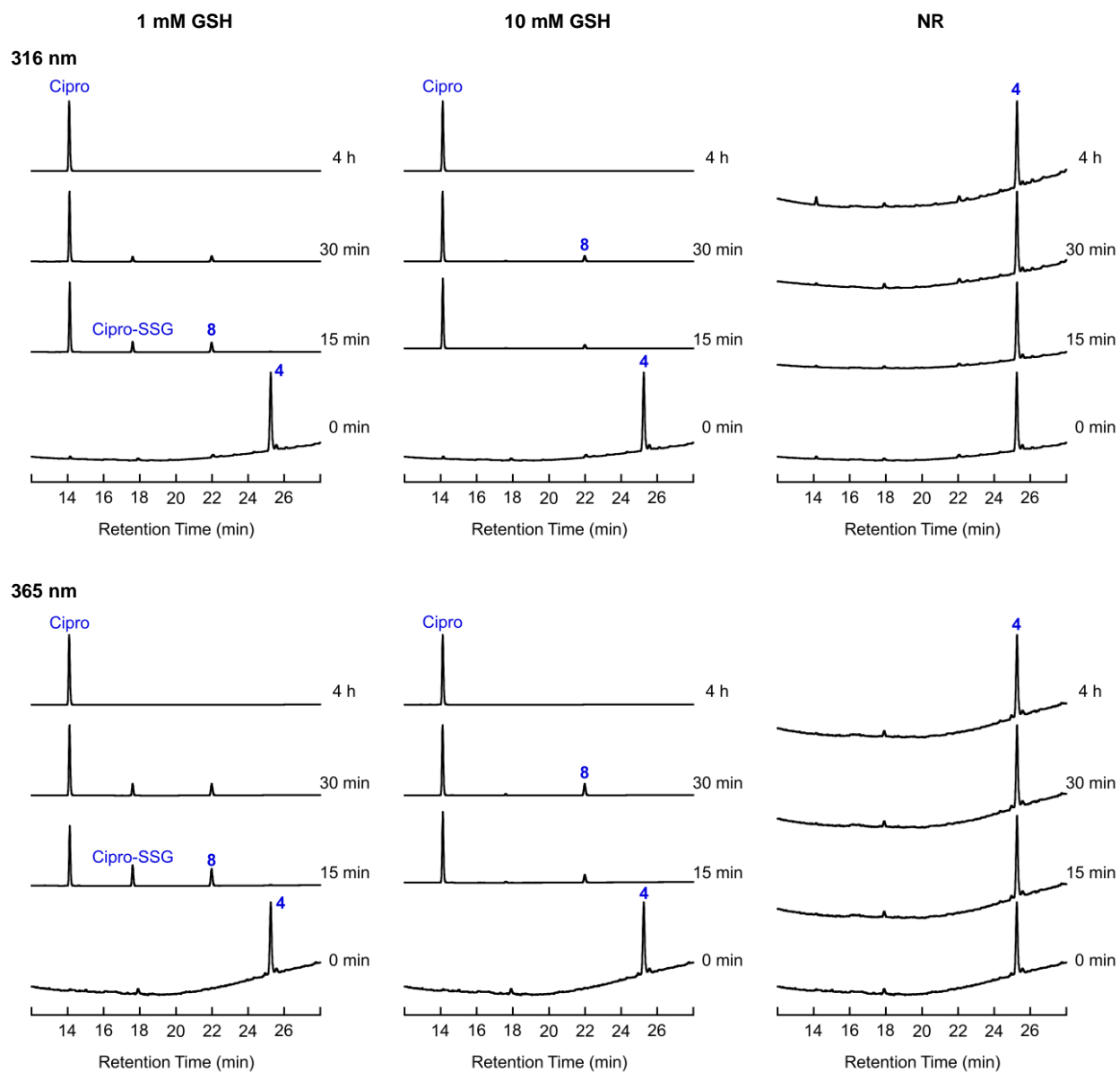


Fig. S6 Cleavage of Cipro–SSEt **4** by GSH at pH 9.0. Analytical HPLC traces of 100 μ M Cipro–SSEt incubated with 1 or 10 mM GSH in 75 mM Tris-HCl, pH 9.0 for the indicated time; aliquots were quenched with acid. Absorbance monitored at 316 nm (top panel) and 365 nm (bottom panel); NR, no-reductant control.

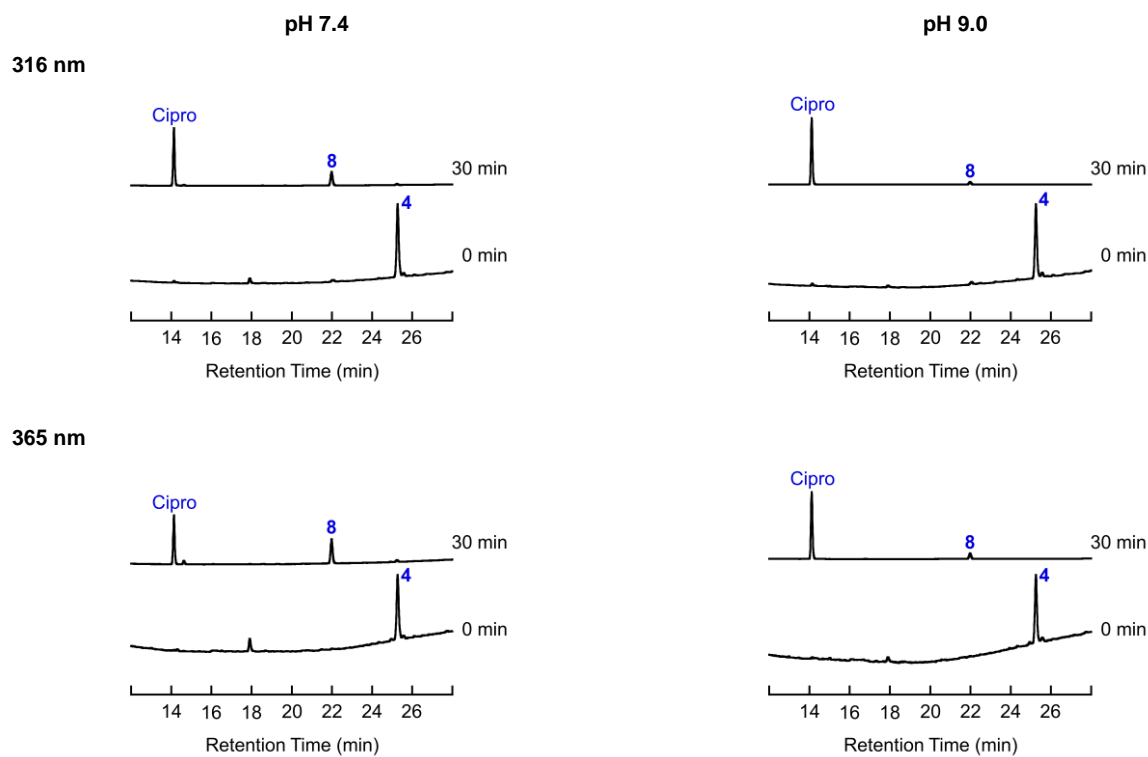


Fig. S7 Cleavage of Cipro–SSEt **4** by TCEP at pH 7.4 and pH 9.0. Analytical HPLC traces of 100 μ M Cipro–SSEt incubated with 1 mM TCEP in 75 mM Tris-HCl, pH 7.4 or 9.0 for the indicated time; aliquots were quenched with acid. Absorbance monitored at 316 nm (top panel) and 365 nm (bottom panel).

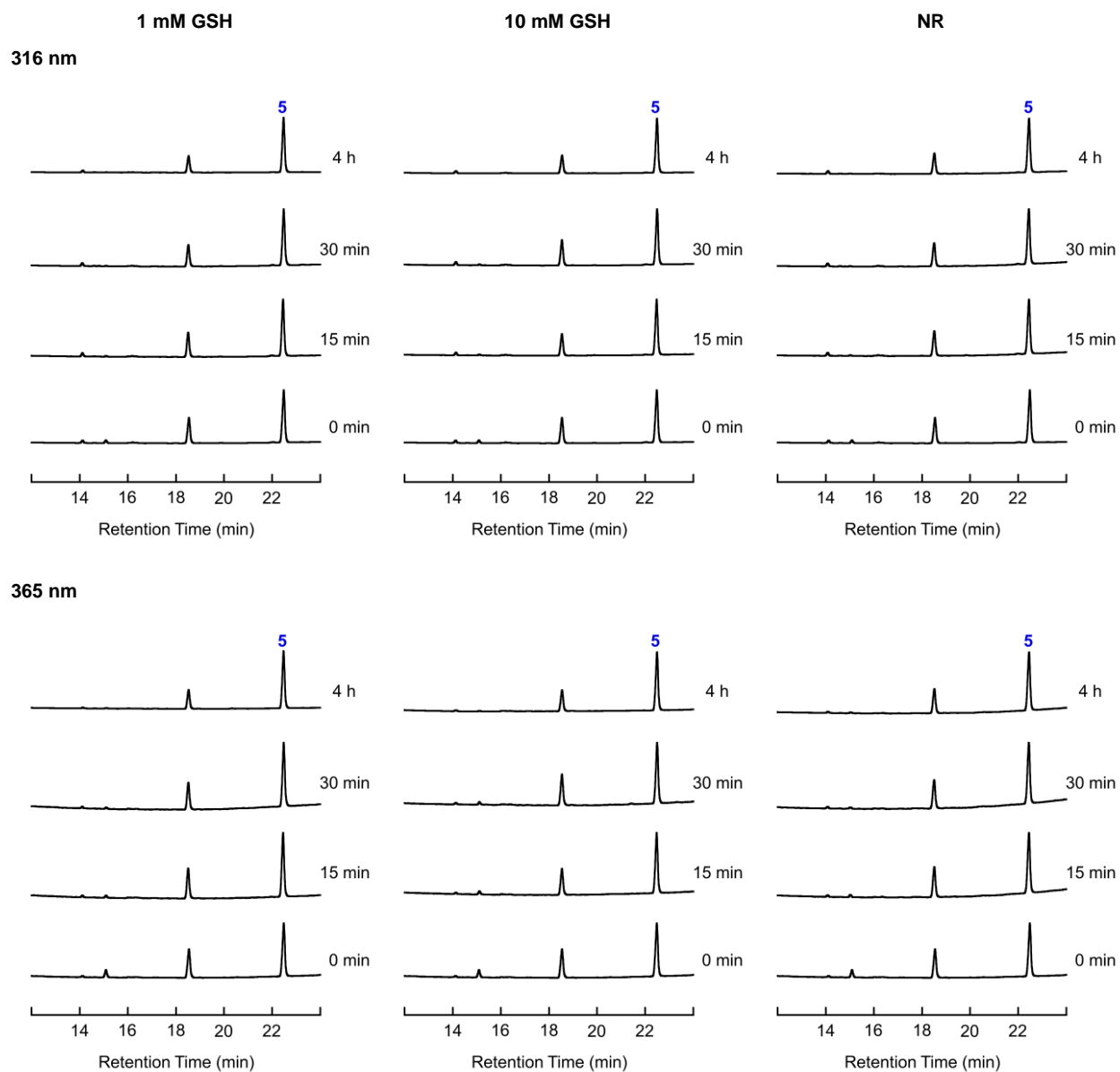


Fig. S8 Incubation of Cipro-SMe **5** with GSH at pH 7.4. Analytical HPLC traces of 100 μ M Cipro-SMe incubated with 1 or 10 mM GSH in 75 mM Tris-HCl, pH 7.4 for the indicated time; aliquots were quenched with acid. Absorbance monitored at 316 nm (top panel) and 365 nm (bottom panel); NR, no-reductant control. When dissolved in Tris buffer, compound **5** elutes as two distinct peaks.

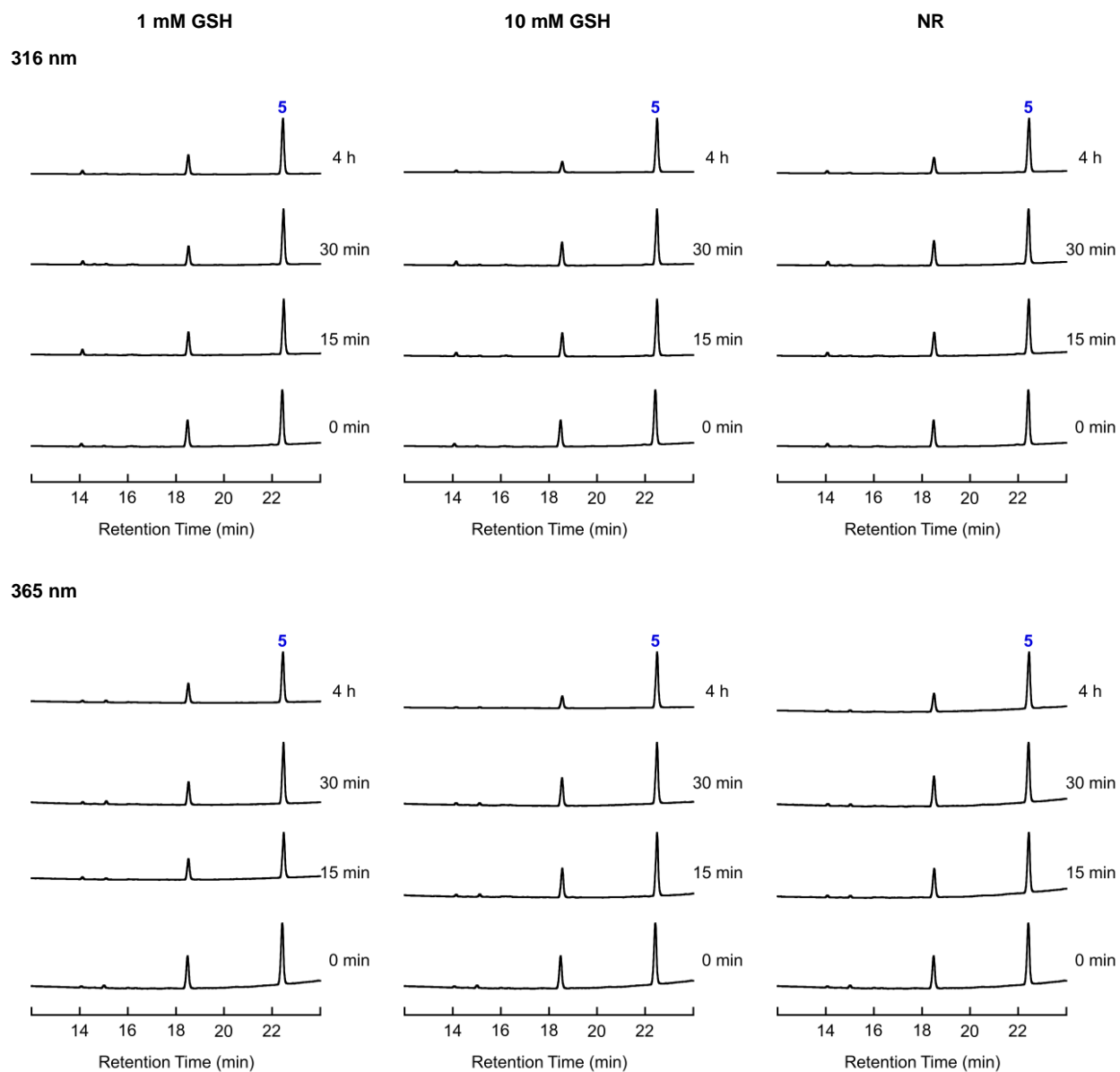


Fig. S9 Incubation of Cipro-SMe **5** with GSH at pH 9.0. Analytical HPLC traces of 100 μ M Cipro-SMe incubated with 1 or 10 mM GSH in 75 mM Tris-HCl, pH 9.0 for the indicated time; aliquots were quenched with acid. Absorbance monitored at 316 nm (top panel) and 365 nm (bottom panel); NR, no-reductant control. When dissolved in Tris buffer, compound **5** elutes as two distinct peaks.

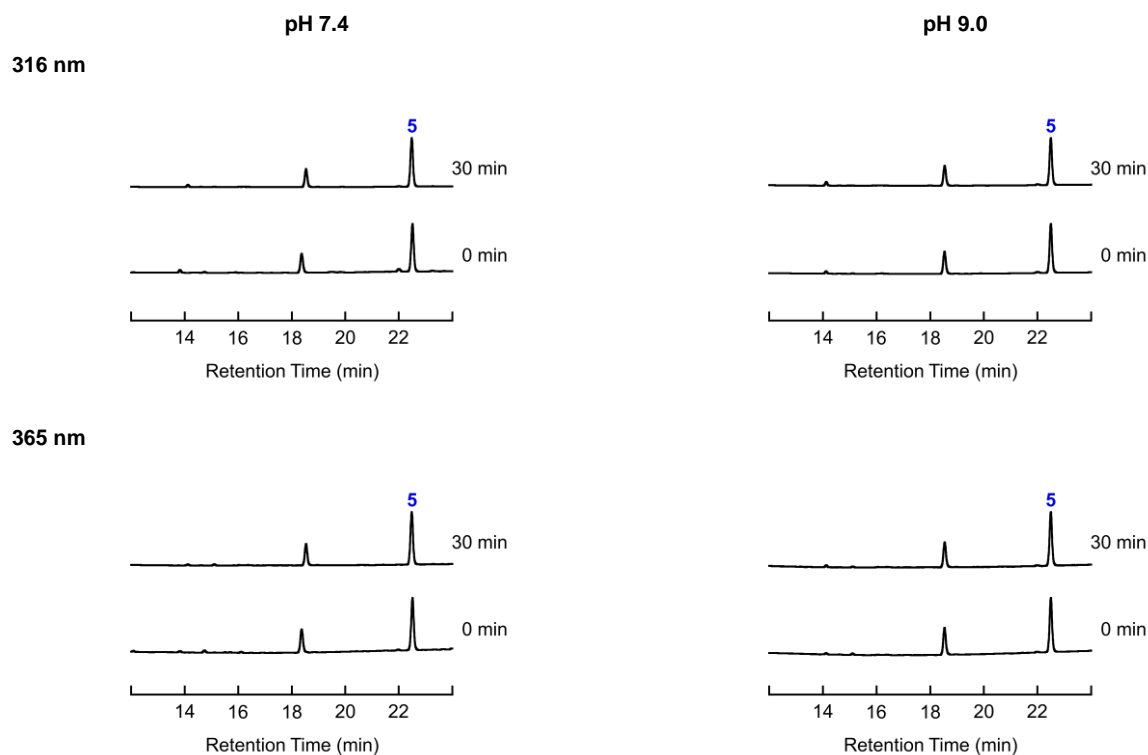


Fig. S10 Incubation of Cipro-SMe **5** with TCEP at pH 7.4 and pH 9.0. Analytical HPLC traces of 100 μ M Cipro-SMe incubated with 1 mM TCEP in 75 mM Tris-HCl, pH 7.4 or 9.0 for the indicated time; aliquots were quenched with acid. Absorbance monitored at 316 nm (top panel) and 365 nm (bottom panel). When dissolved in Tris buffer, compound **5** elutes as two distinct peaks.

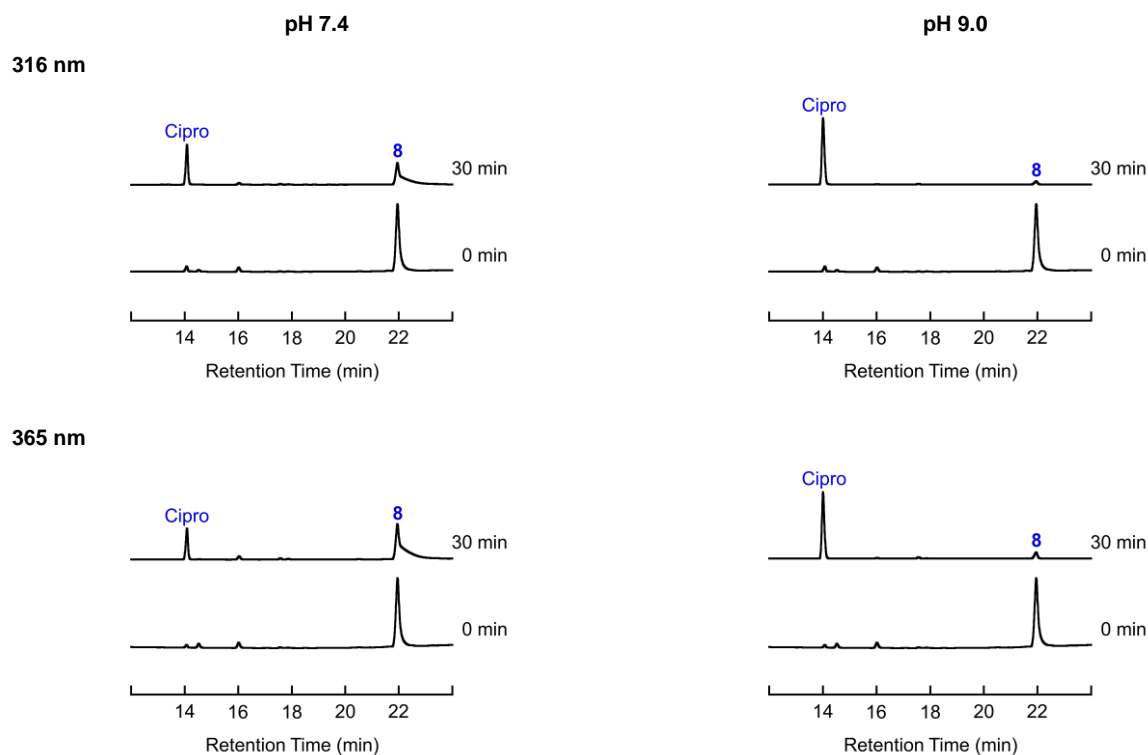


Fig. S11 Incubation of Cipro-SH **8** with GSH at pH 7.4 and pH 9.0. Analytical HPLC traces of 100 μ M Cipro-SH incubated with 1 mM GSH in 75 mM Tris-HCl, pH 7.4 or 9.0 for the indicated time; aliquots were quenched with acid. Absorbance monitored at 316 nm (top panel) and 365 nm (bottom panel).

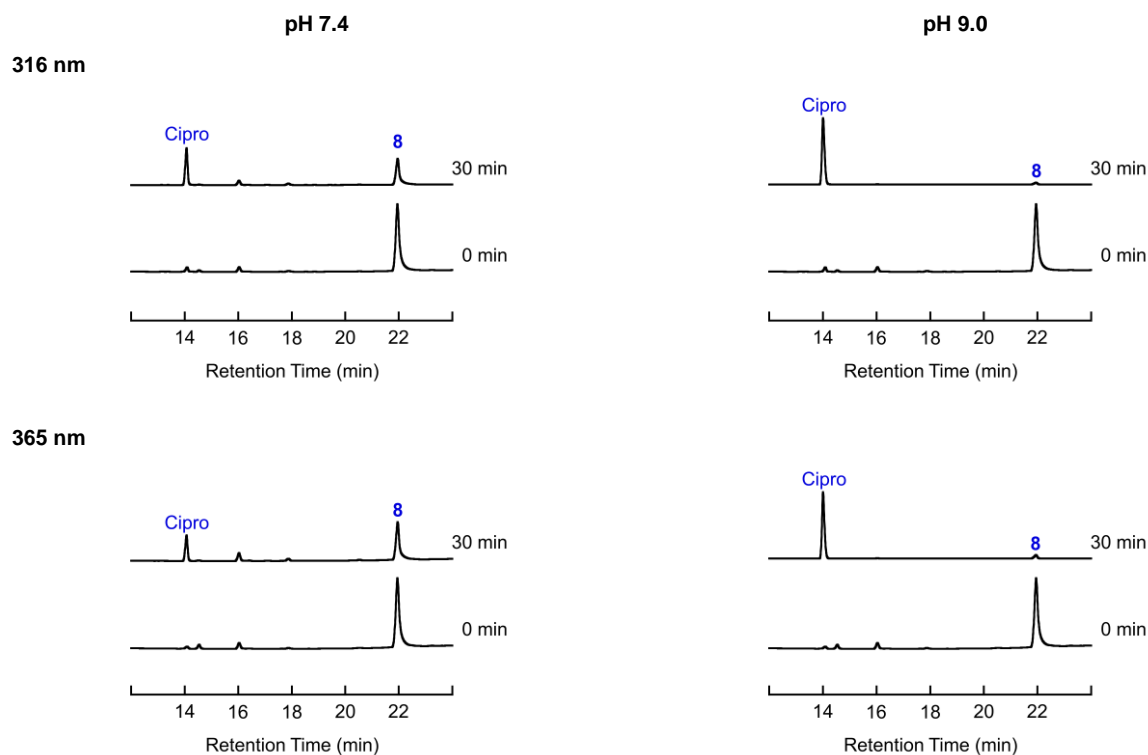


Fig. S12 Incubation of Cipro-SH **8** with TCEP at pH 7.4 and pH 9.0. Analytical HPLC traces of 100 μ M Cipro-SH incubated with 1 mM TCEP in 75 mM Tris-HCl, pH 7.4 or 9.0 for the indicated time; aliquots were quenched with acid. Absorbance monitored at 316 nm (top panel) and 365 nm (bottom panel).

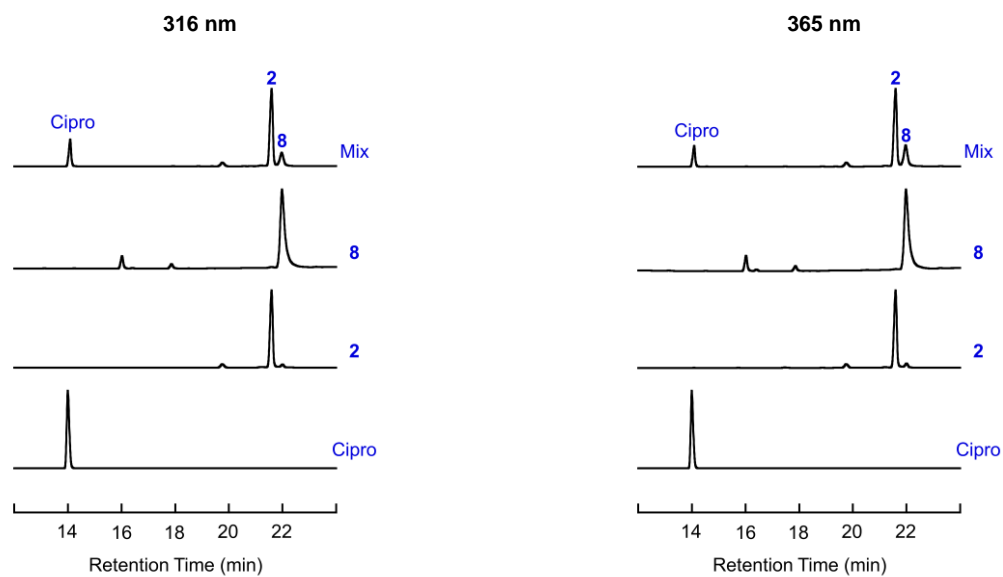


Fig. S13 Analytical HPLC traces of Ent-SS-Cipro **2**, Cipro-SH **8** and ciprofloxacin, and a mixture of those compounds; absorbance monitored at 316 nm and 365 nm.

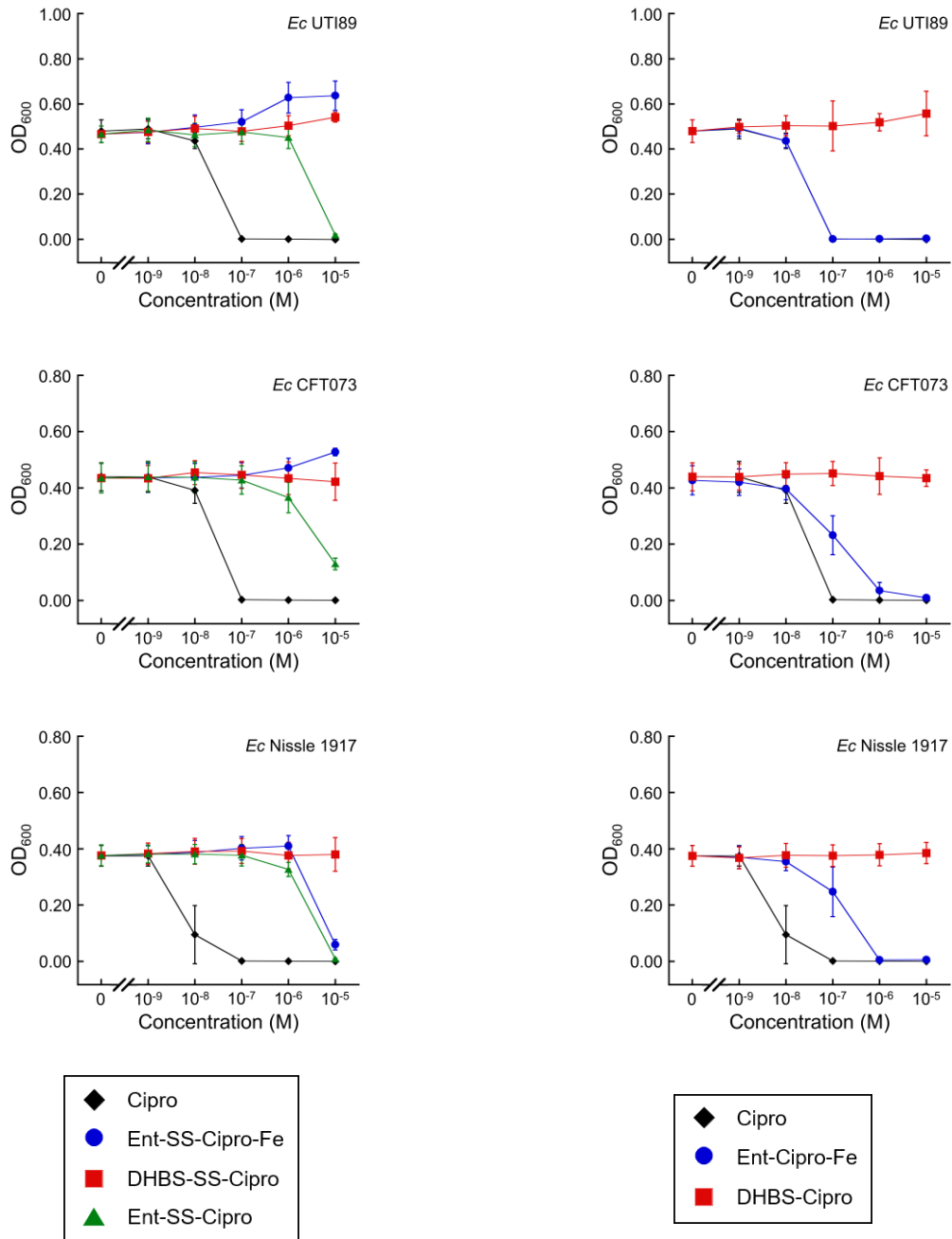


Fig. S14 Antibacterial activity of Ent-SS-Cipro 2 and DHBS-SS-Cipro 3 (left panel), in comparison with Ent-Cipro 1 and DHBS-Cipro (right panel), against uropathogenic and non-pathogenic *E. coli* strains that express IroD in modified M9 medium (mean \pm SDM, $n = 3$). In the case of ferric conjugates, the siderophores were pre-loaded with 0.9 equiv Fe(III) (blue traces).

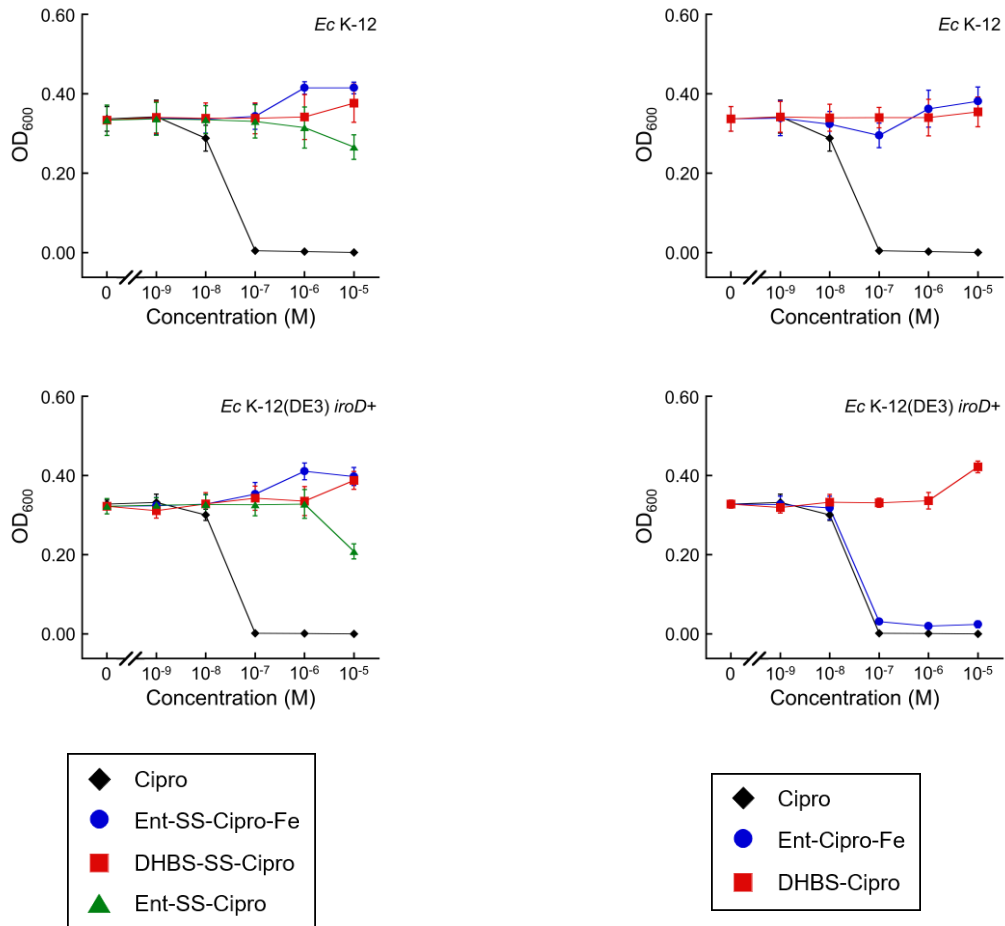


Fig. S15 Antibacterial activity of Ent-SS-Cipro **2** and DHBS-SS-Cipro **3** (left panel), in comparison with Ent-Cipro **1** and DHBS-Cipro (right panel), against *E. coli* K-12, wild-type and complemented with *iroD*, in modified M9 medium (mean \pm SDM, $n = 3$). In the case of ferric conjugates, the siderophores were pre-loaded with 0.9 equiv Fe(III) (blue traces).

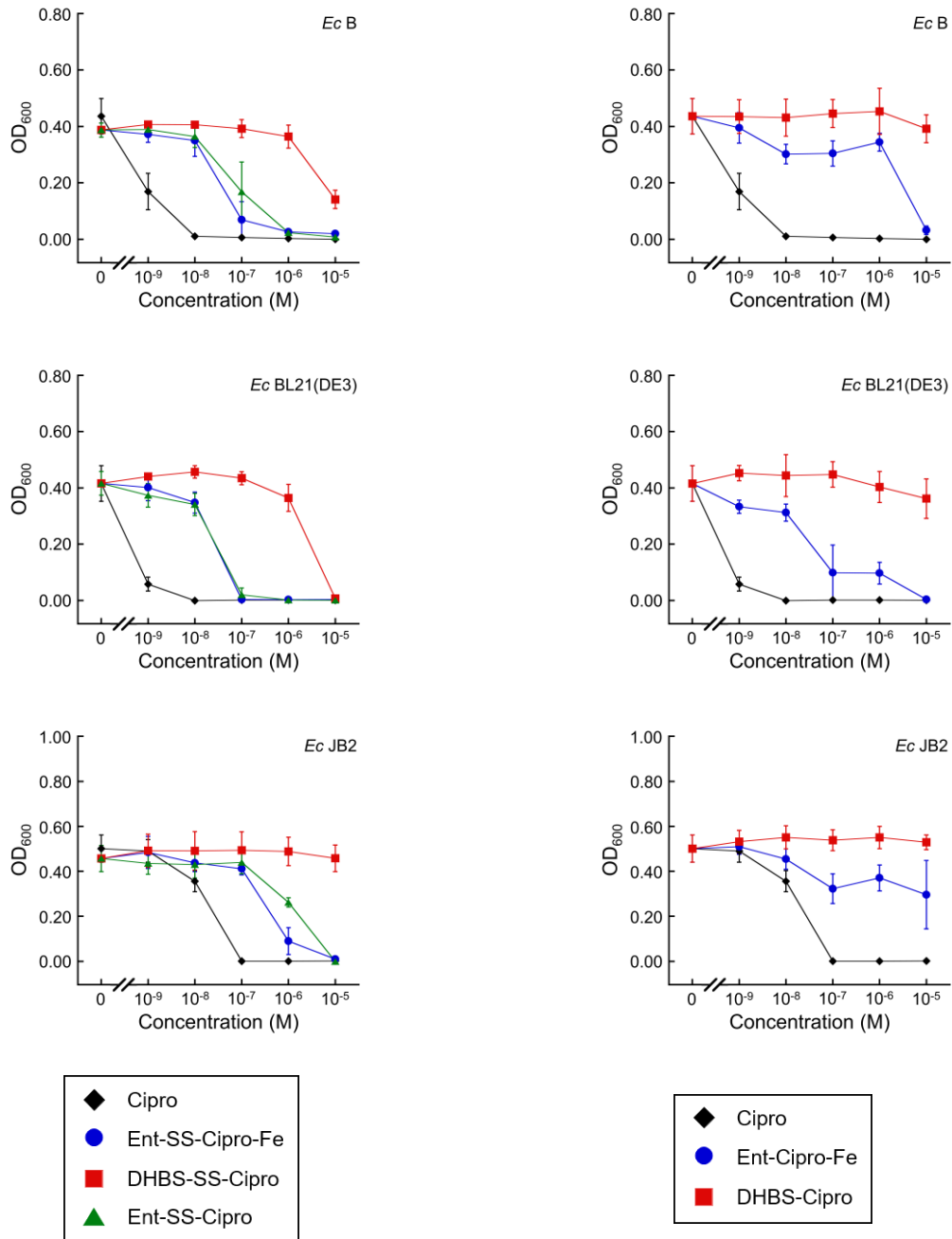


Fig. S16 Antibacterial activity of Ent-SS-Cipro **2** and DHBS-SS-Cipro **3** (left panel), in comparison with Ent-Cipro **1** and DHBS-Cipro (right panel), against non-pathogenic *E. coli* strains that do not express IroD in modified M9 medium (mean \pm SDM, $n = 3$). In the case of ferric conjugates, the siderophores were pre-loaded with 0.9 equiv Fe(III) (blue traces).

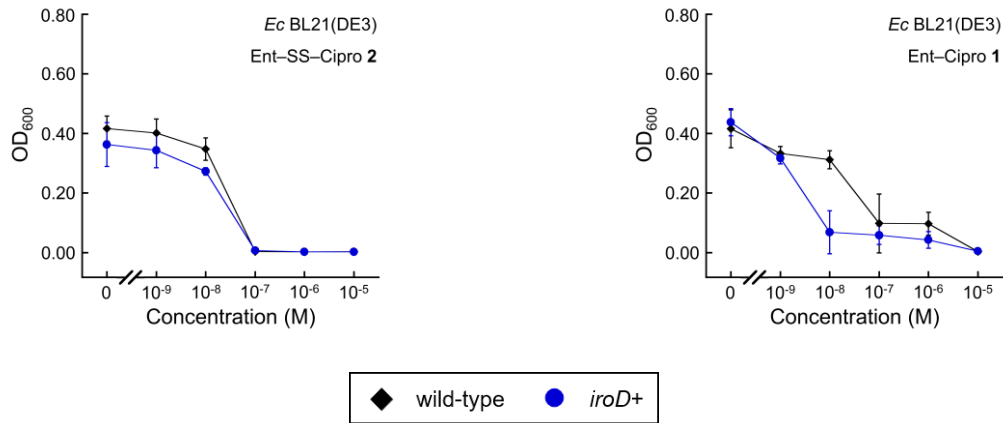


Fig. S17 Antibacterial activity of ferric Ent-SS-Cipro 2 (left) in comparison with ferric Ent-Cipro 1 (right) against *E. coli* BL21(DE3), wild-type or complemented with *iroD*, in modified M9 medium (mean \pm SDM, $n = 3$). The conjugates were pre-loaded with 0.9 equiv Fe(III).

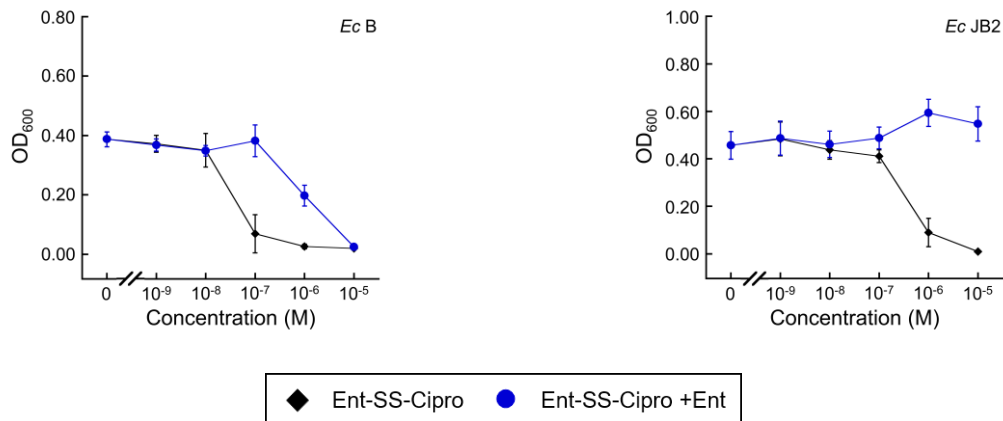


Fig. S18 Antibacterial activity of ferric Ent-SS-Cipro 2 against *E. coli* B and JB2 in the absence and presence of Ent in modified M9 medium (mean \pm SDM, $n = 3$). For co-treatment, a 1:1 molar ratio of apo Ent and ferric 2 was employed.

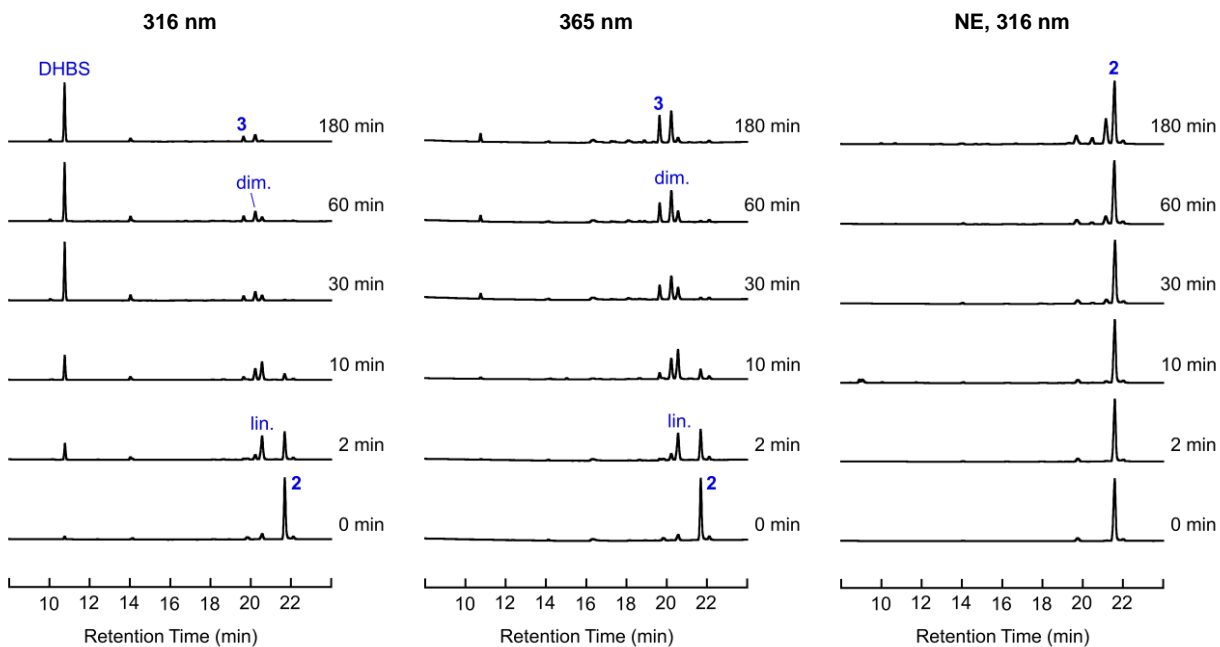


Fig. S19 Hydrolysis of Ent-SS-Cipro **2** by IroD to the linear trimer (lin.), the dimer (dim.), DHBS-SS-Cipro **3**, and DHBS. Analytical HPLC traces of 300 μ M Ent-SS-Cipro incubated with 0.3 μ M IroD in 75 mM Tris-HCl, pH 8.0 for the indicated time; aliquots were quenched with acid. Absorbance monitored at 316 nm and 365 nm; NE, no-enzyme control.

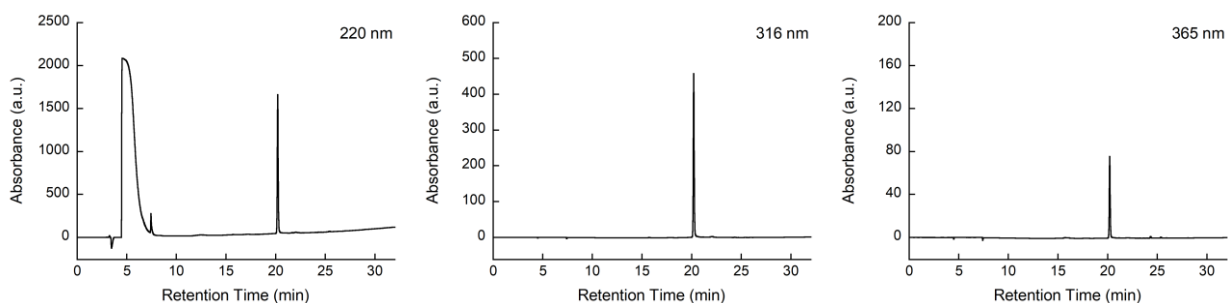


Fig. S20 Analytical HPLC traces of purified Ent-Cipro **1**; absorbance monitored at 220 nm, 316 nm, and 365 nm. The compound was dissolved in Milli-Q H₂O, 10% DMSO.

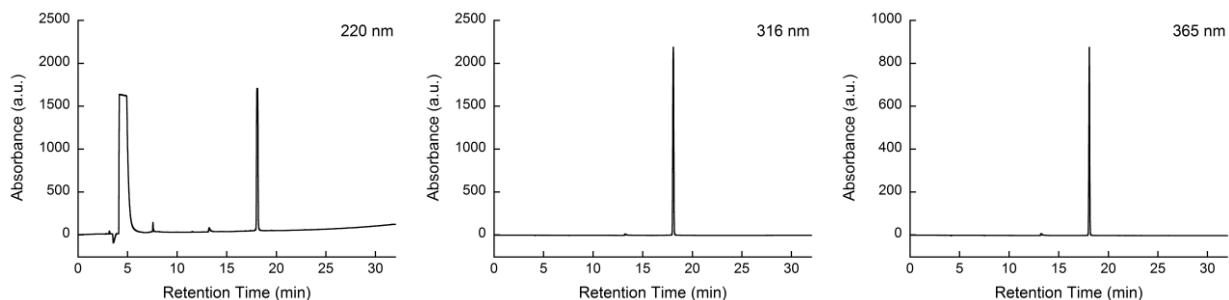


Fig. S21 Analytical HPLC traces of purified DHBS-Cipro; absorbance monitored at 220 nm, 316 nm, and 365 nm. The compound was dissolved in Milli-Q H₂O, 10% DMSO.

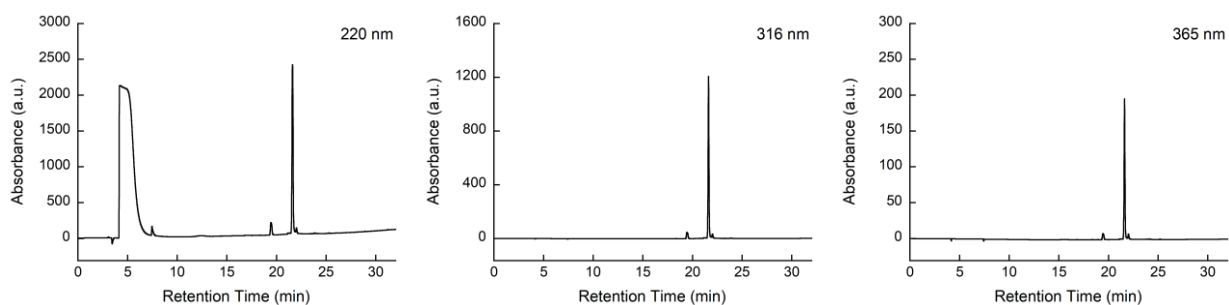


Fig. S22 Analytical HPLC traces of purified Ent-SS-Cipro 2; absorbance monitored at 220 nm, 316 nm, and 365 nm. The compound was dissolved in H₂O, 10% DMSO.

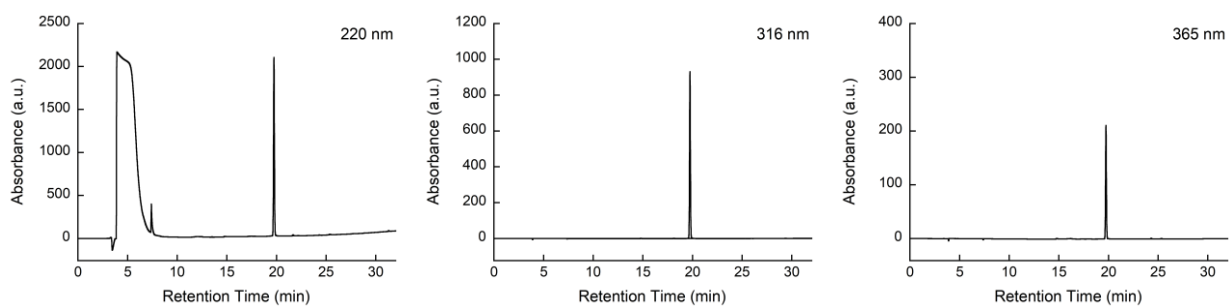


Fig. S23 Analytical HPLC traces of purified DHBS-SS-Cipro 3; absorbance monitored at 220 nm, 316 nm, and 365 nm. The compound was dissolved in Milli-Q H₂O, 10% DMSO.

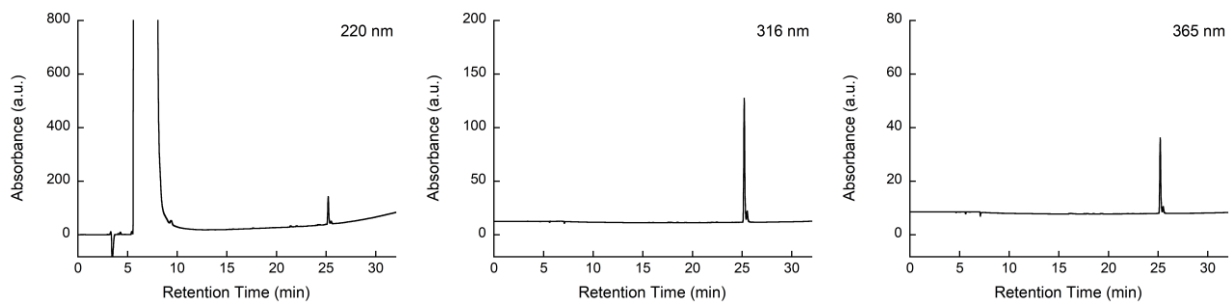


Fig. S24 Analytical HPLC traces of purified Cipro-SSEt **4**; absorbance monitored at 220 nm, 316 nm, and 365 nm. The compound was dissolved in Milli-Q H₂O, 5% DMF.

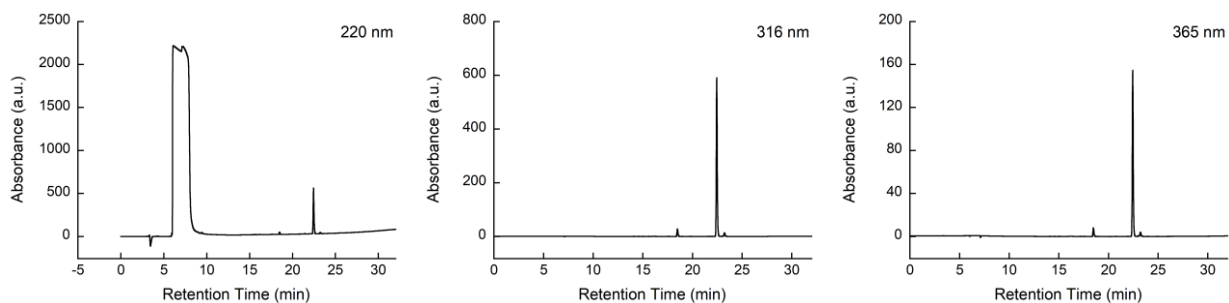


Fig. S25 Analytical HPLC traces of purified Cipro-SMe **5**; absorbance monitored at 220 nm, 316 nm, and 365 nm. The compound was dissolved in Milli-Q H₂O, 5% DMF.

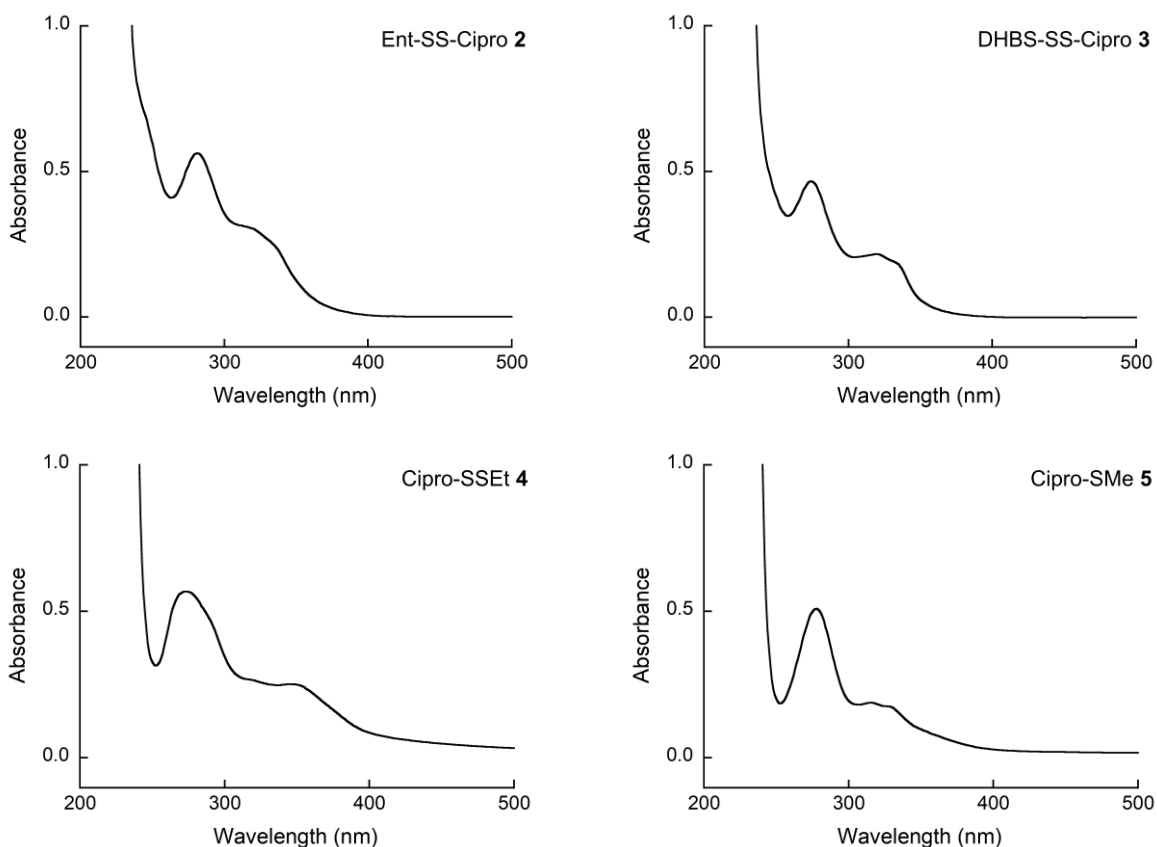


Fig. S26 Optical absorption spectra of the ciprofloxacin derivatives. The stock solutions were diluted with Milli-Q H₂O.

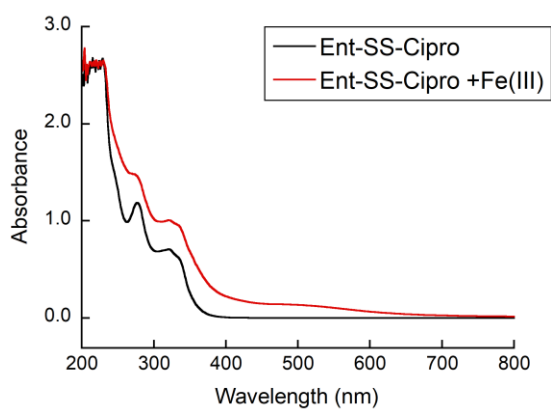


Fig. S27 Optical absorption spectra of apo and ferric Ent-SS-Cipro 2. The DMSO stock was diluted into 75 mM Tris-HCl, pH 8.0 to 100 μ M). The spectra were collected before and after addition of 100 μ M FeCl₃. After addition of Fe(III), the sample was incubated at r.t. for 5 min before the spectrum was collected.

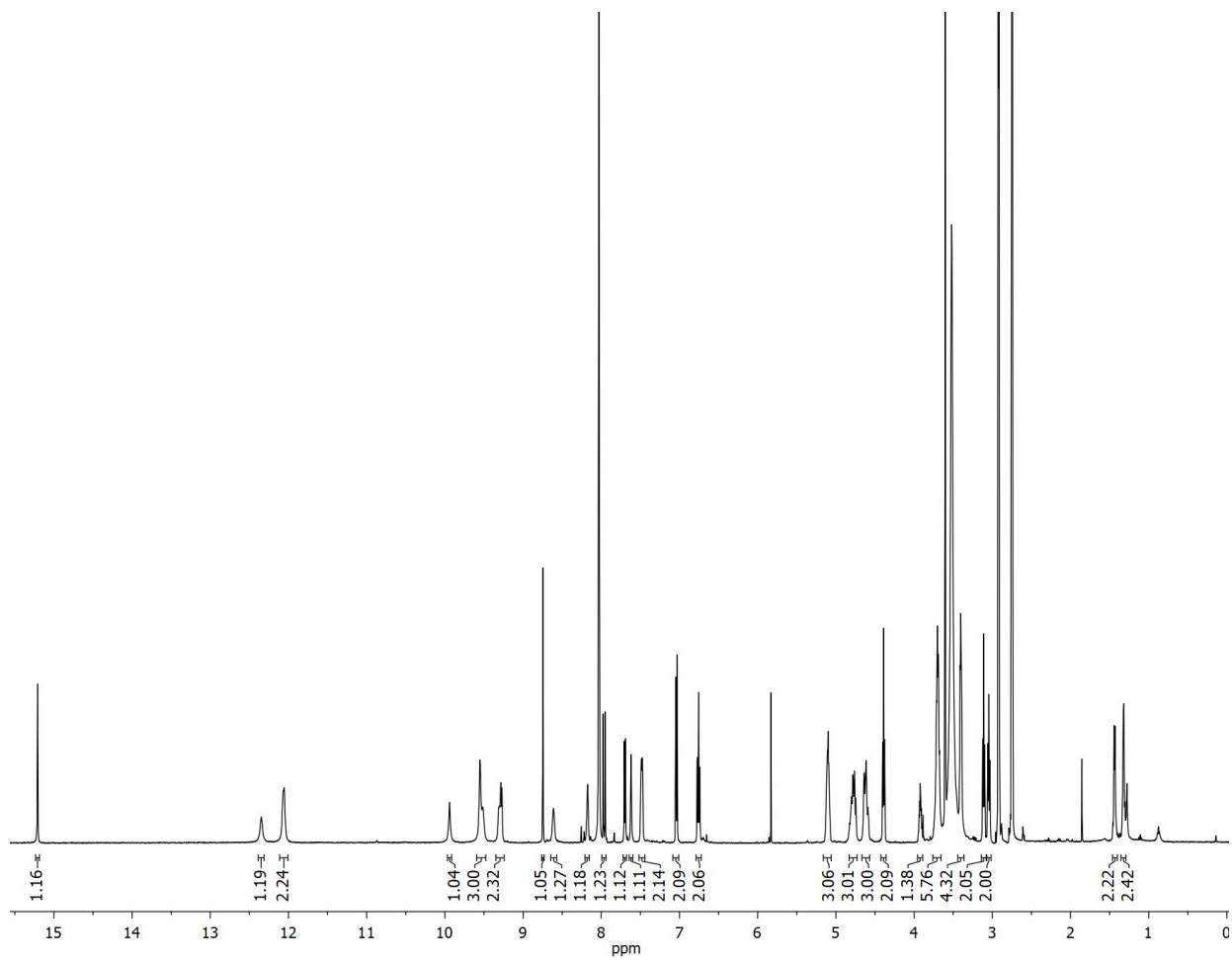


Fig. S28 ^1H NMR (DMF- d_7 , 500 MHz) of **2**.

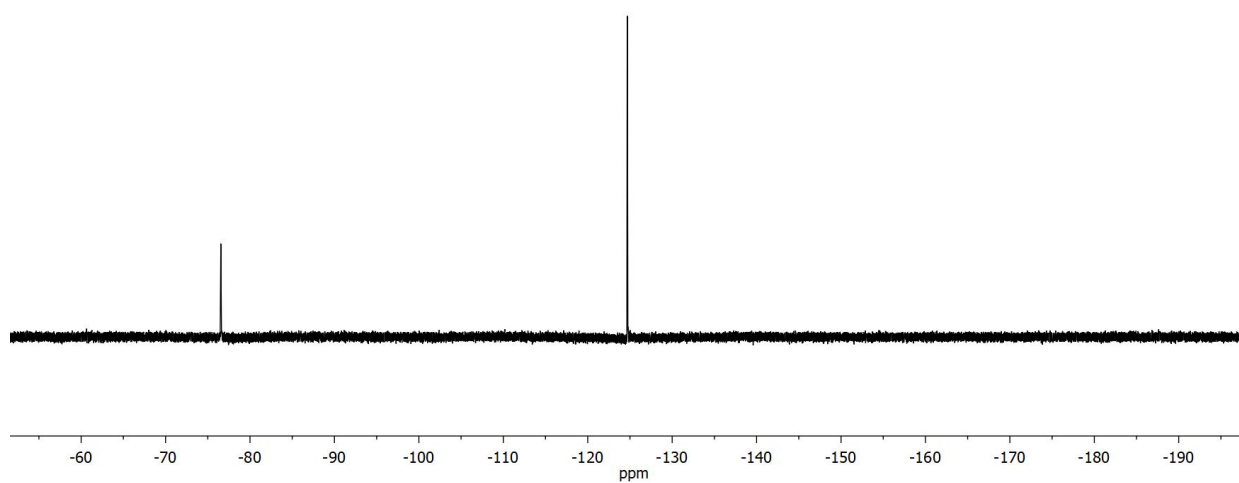


Fig. S29 ^{19}F NMR (DMF- d_7 , 470 MHz) of **2**.

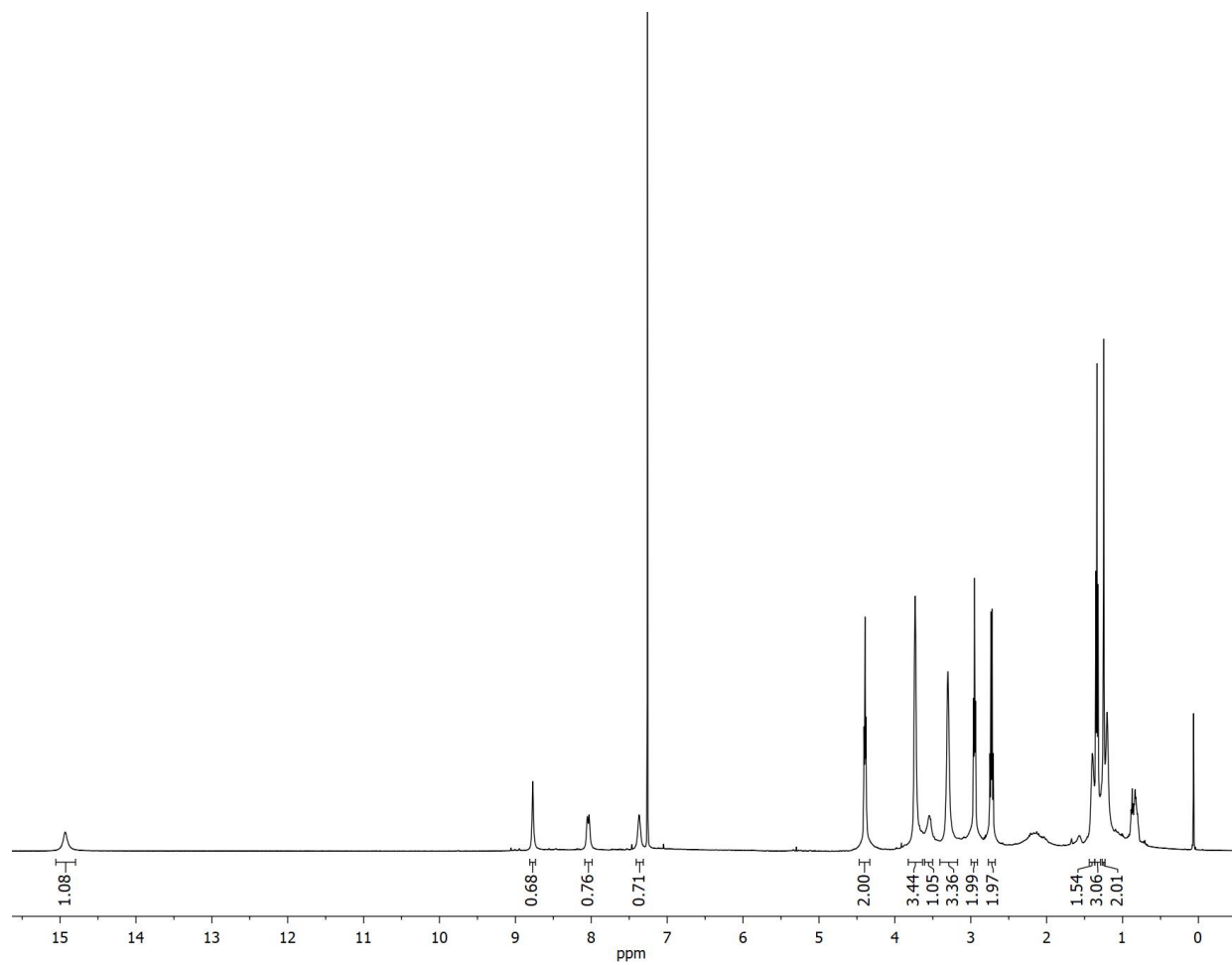


Fig. S30 ^1H NMR (CDCl_3 , 500 MHz) of **4**.

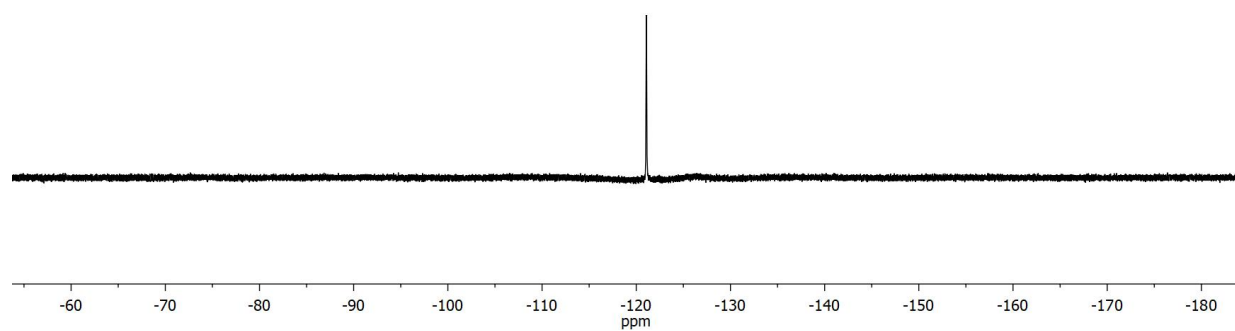


Fig. S31 ^{19}F NMR (CDCl_3 , 470 MHz) of **4**.

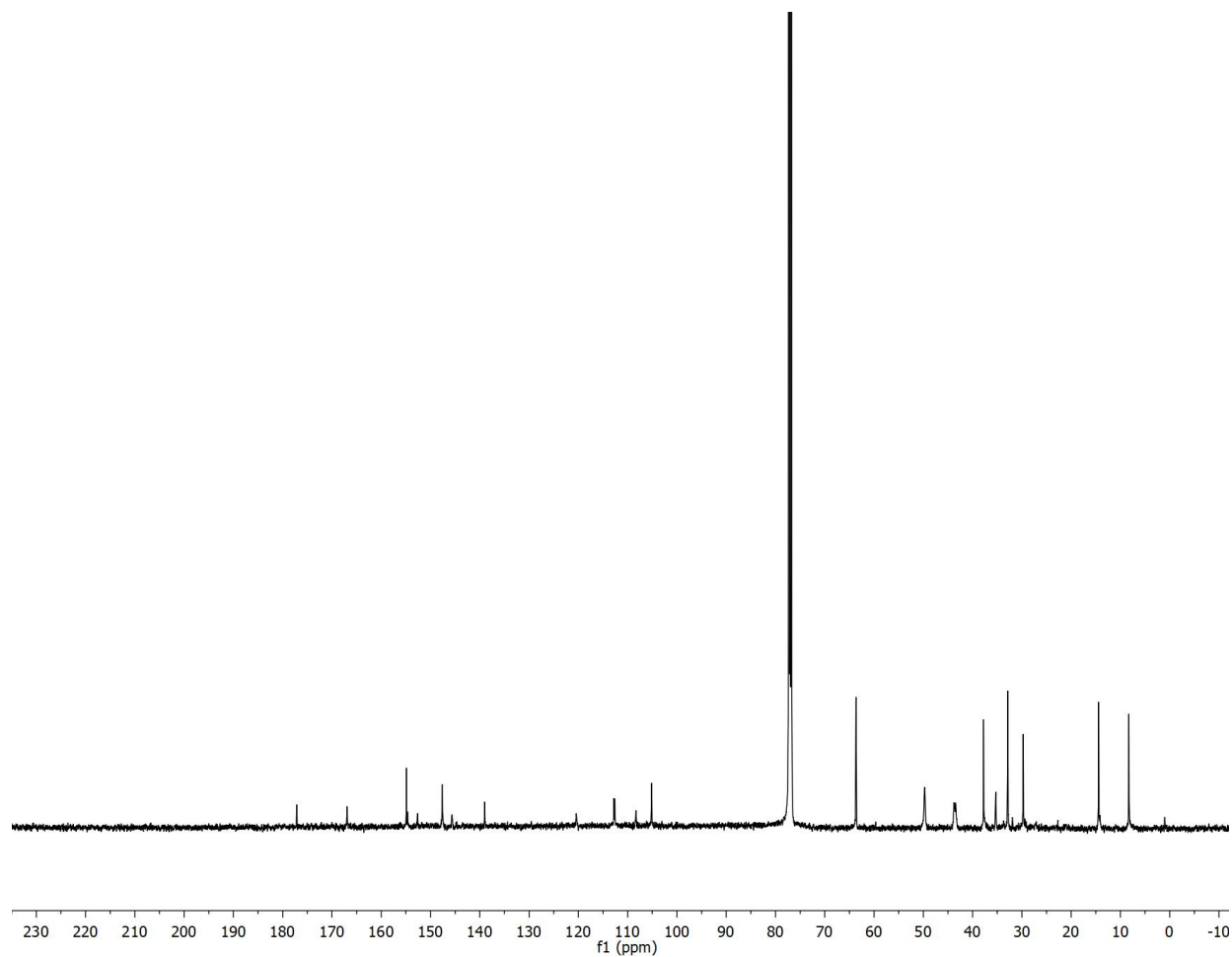


Fig. S32 $^{13}\text{C}\{^1\text{H}\}$ NMR (CDCl_3 , 125 MHz) of **4**.

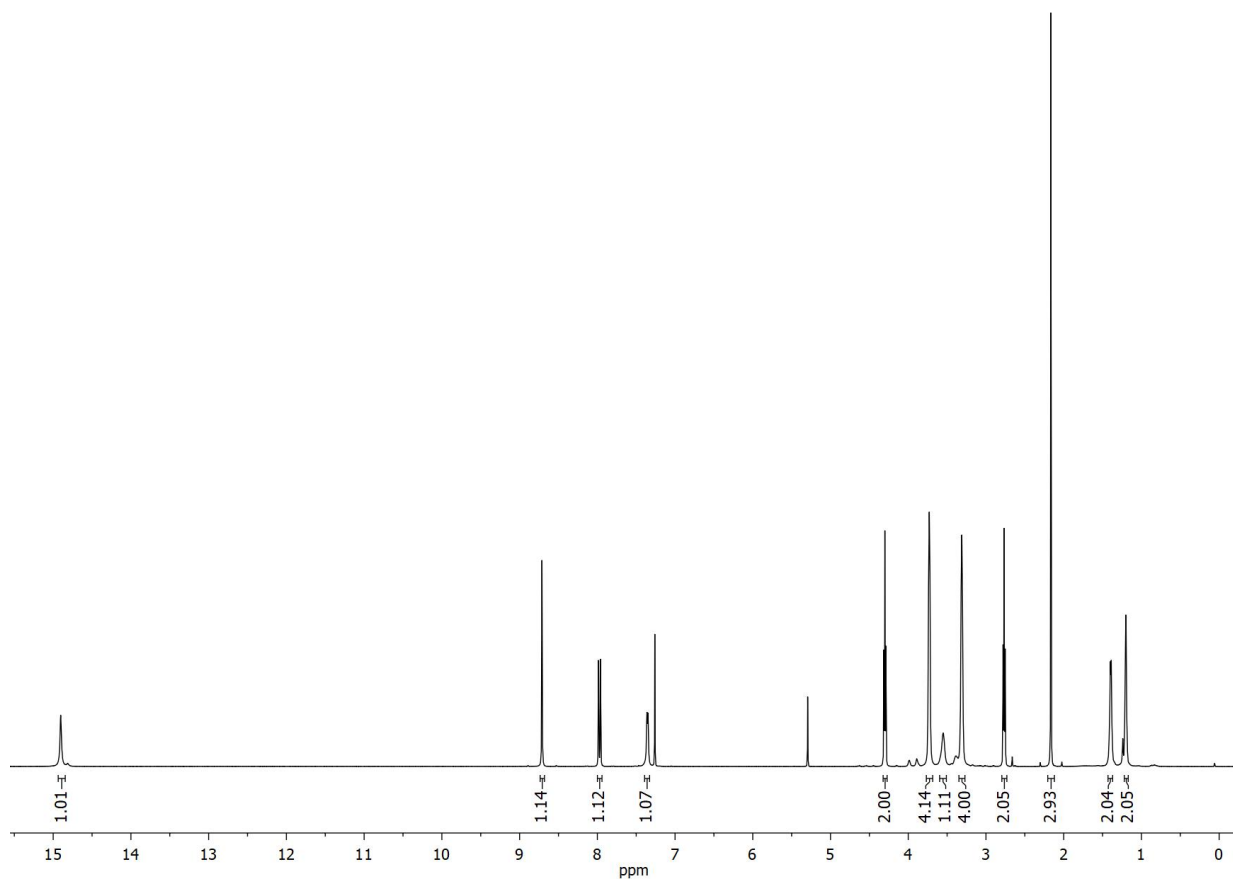


Fig. S33 ¹H NMR (CDCl₃, 500 MHz) of **5**.

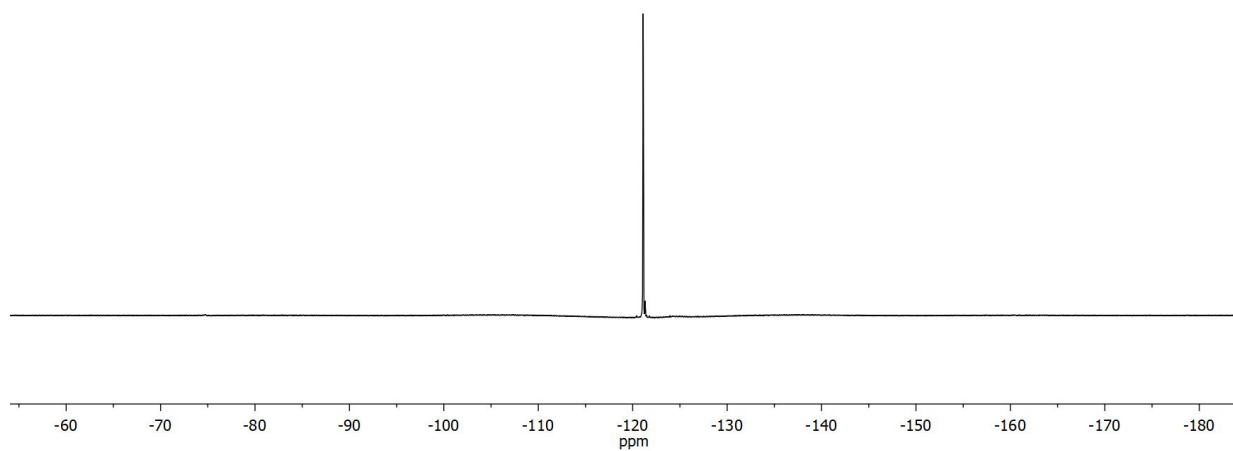


Fig. S34 ^{19}F NMR (CDCl_3 , 470 MHz) of **5**.

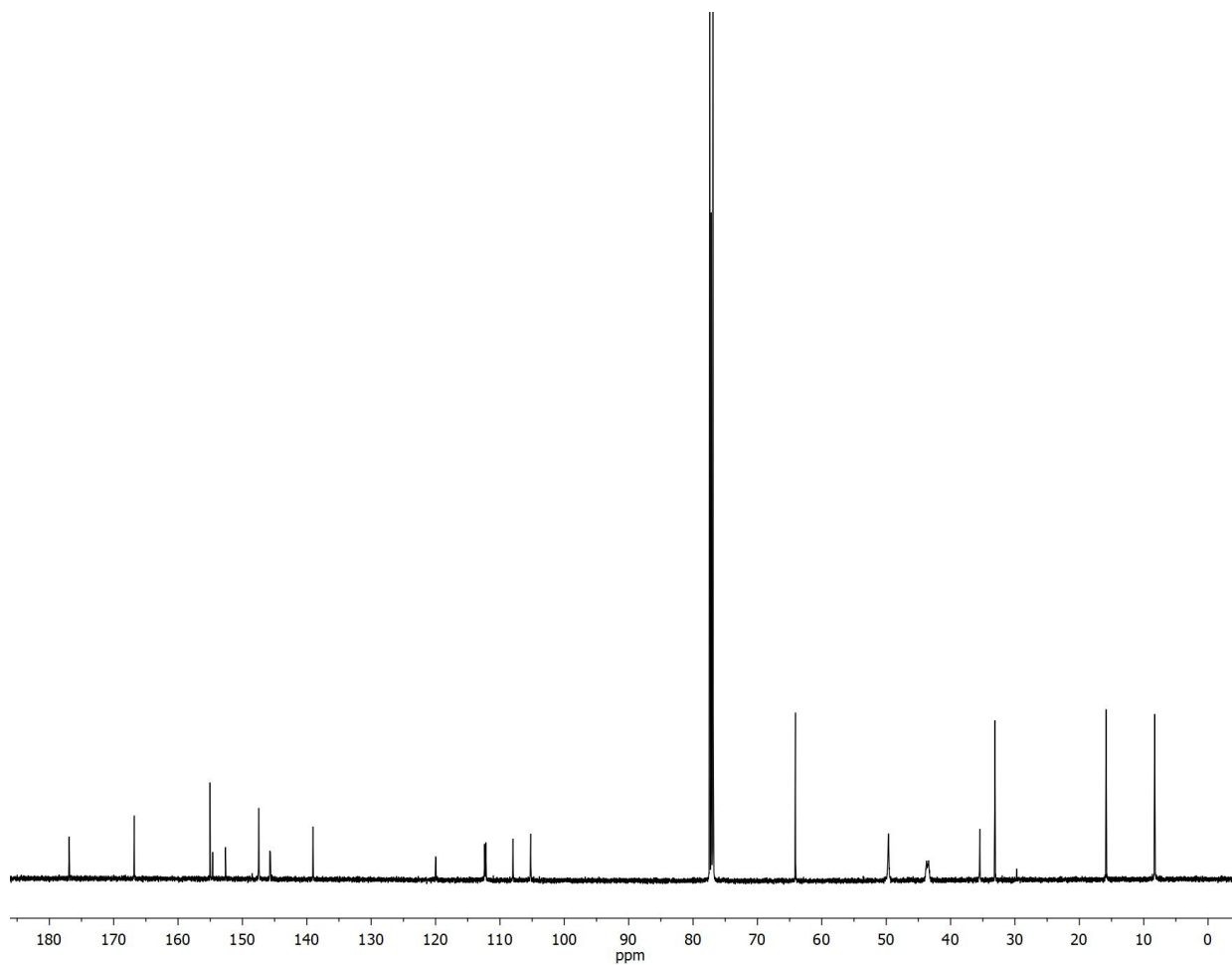


Fig. S35 $^{13}\text{C}\{^1\text{H}\}$ NMR (CDCl_3 , 125 MHz) of **5**.

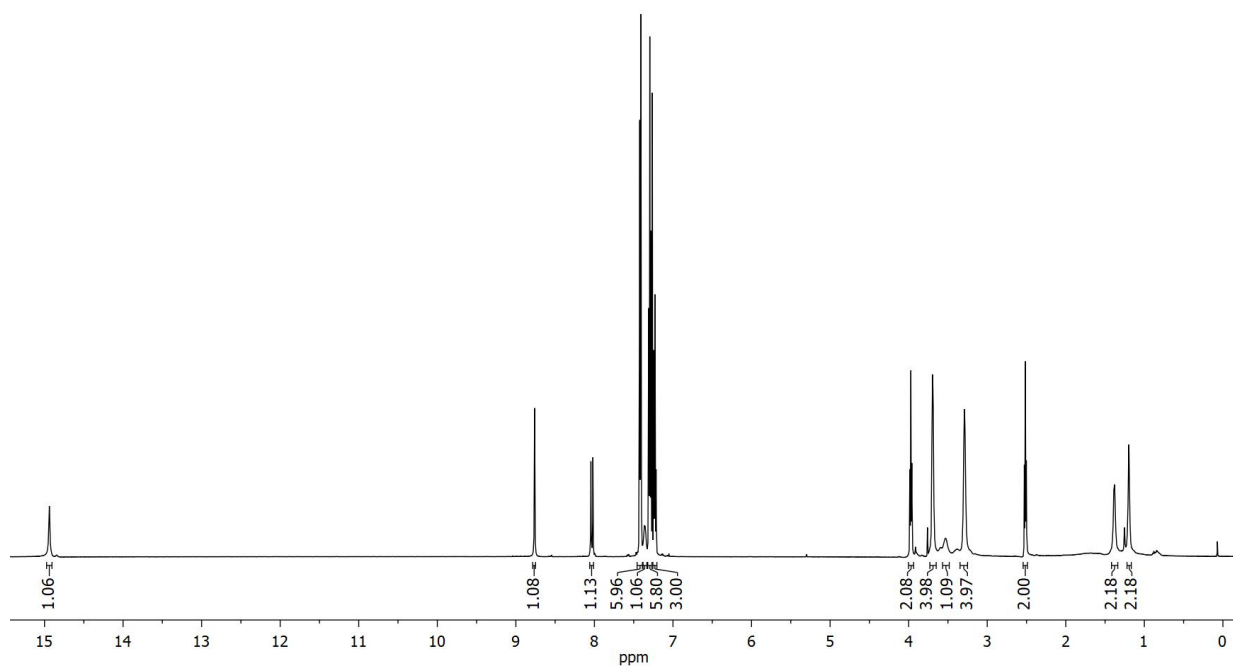


Fig. S36 ^1H NMR (CDCl_3 , 500 MHz) of **7**.

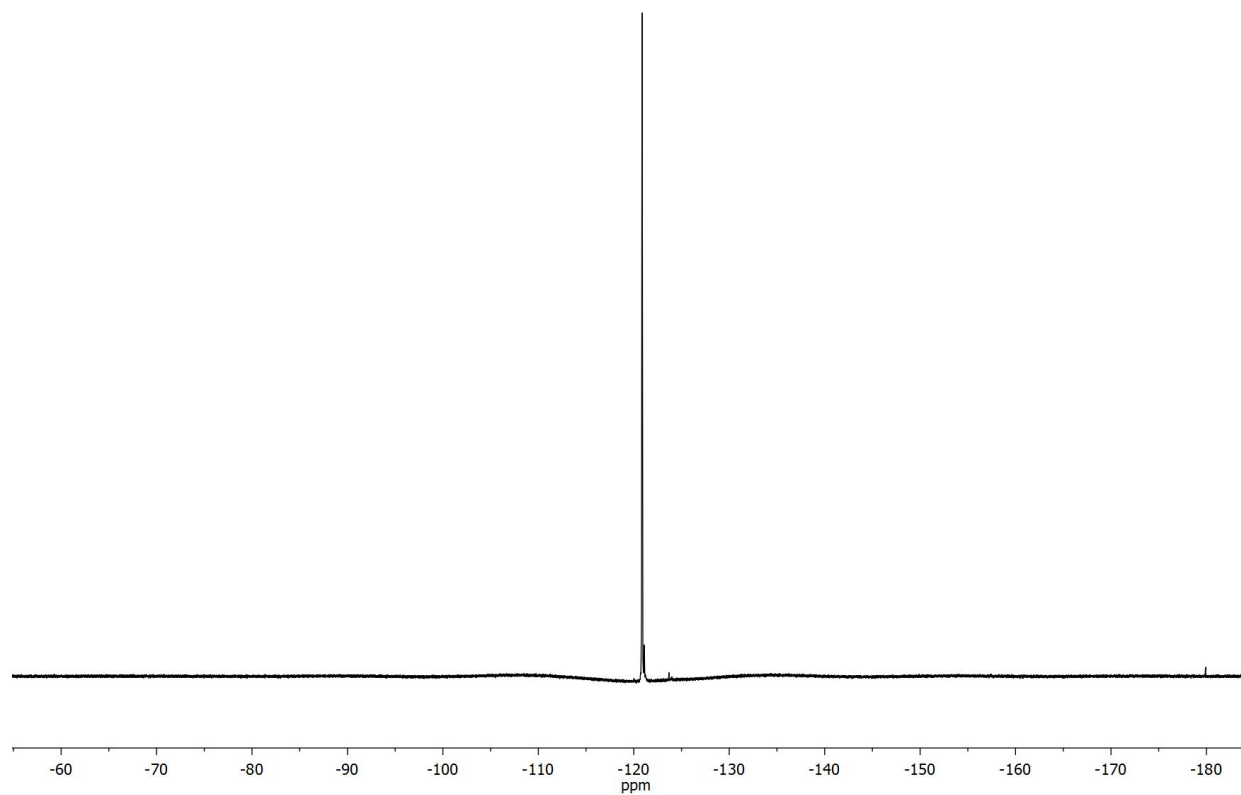


Fig. S37 ^{19}F NMR (CDCl_3 , 470 MHz) of **7**.

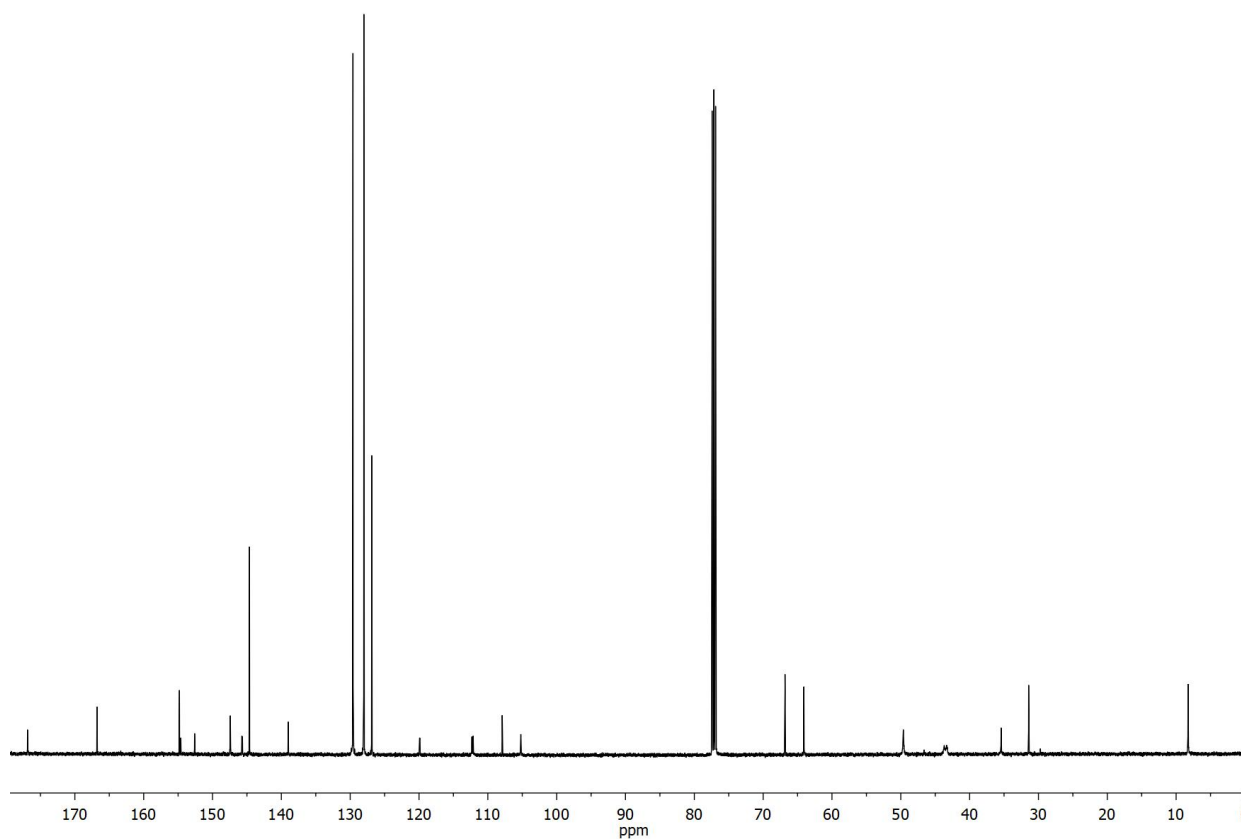


Fig. S38 $^{13}\text{C}\{^1\text{H}\}$ NMR (CDCl_3 , 125 MHz) of **7**.

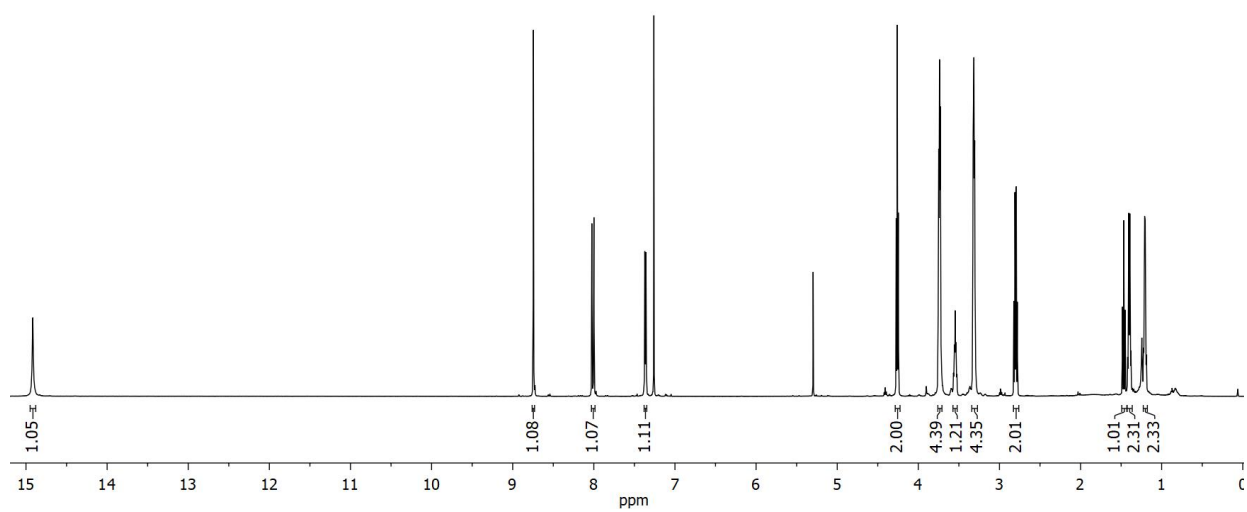


Fig. S39 ^1H NMR (CDCl_3 , 500 MHz) of **8**.

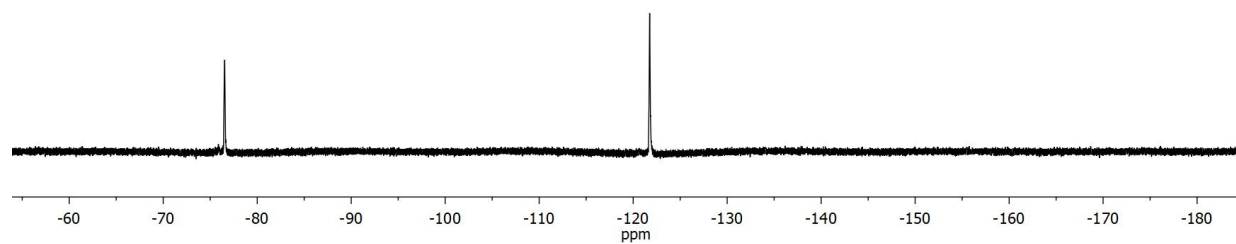


Fig. S40 ^{19}F NMR (CDCl_3 , 470 MHz) of **8**.

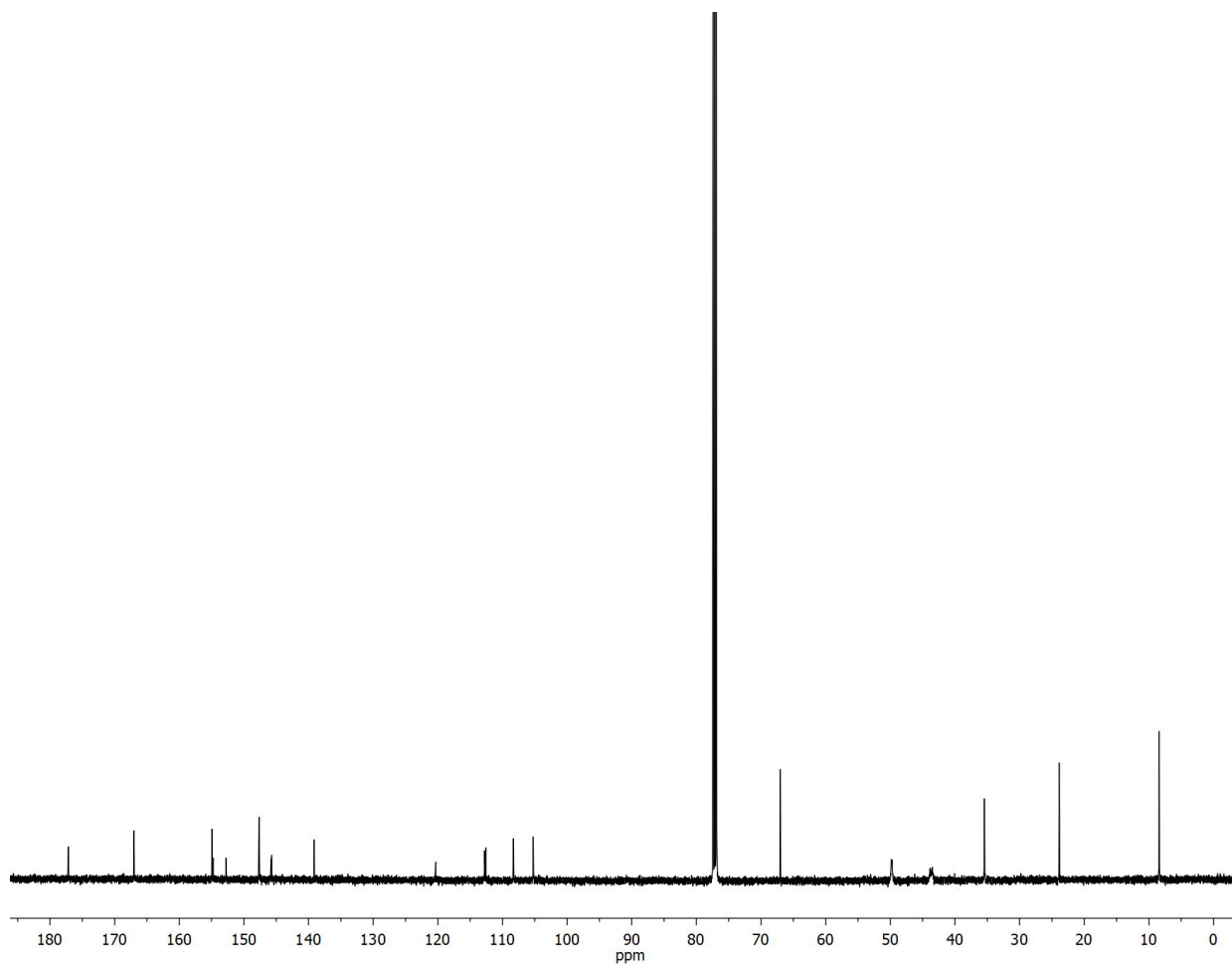


Fig. S41 $^{13}\text{C}\{^1\text{H}\}$ NMR (CDCl_3 , 125 MHz) of **8**.

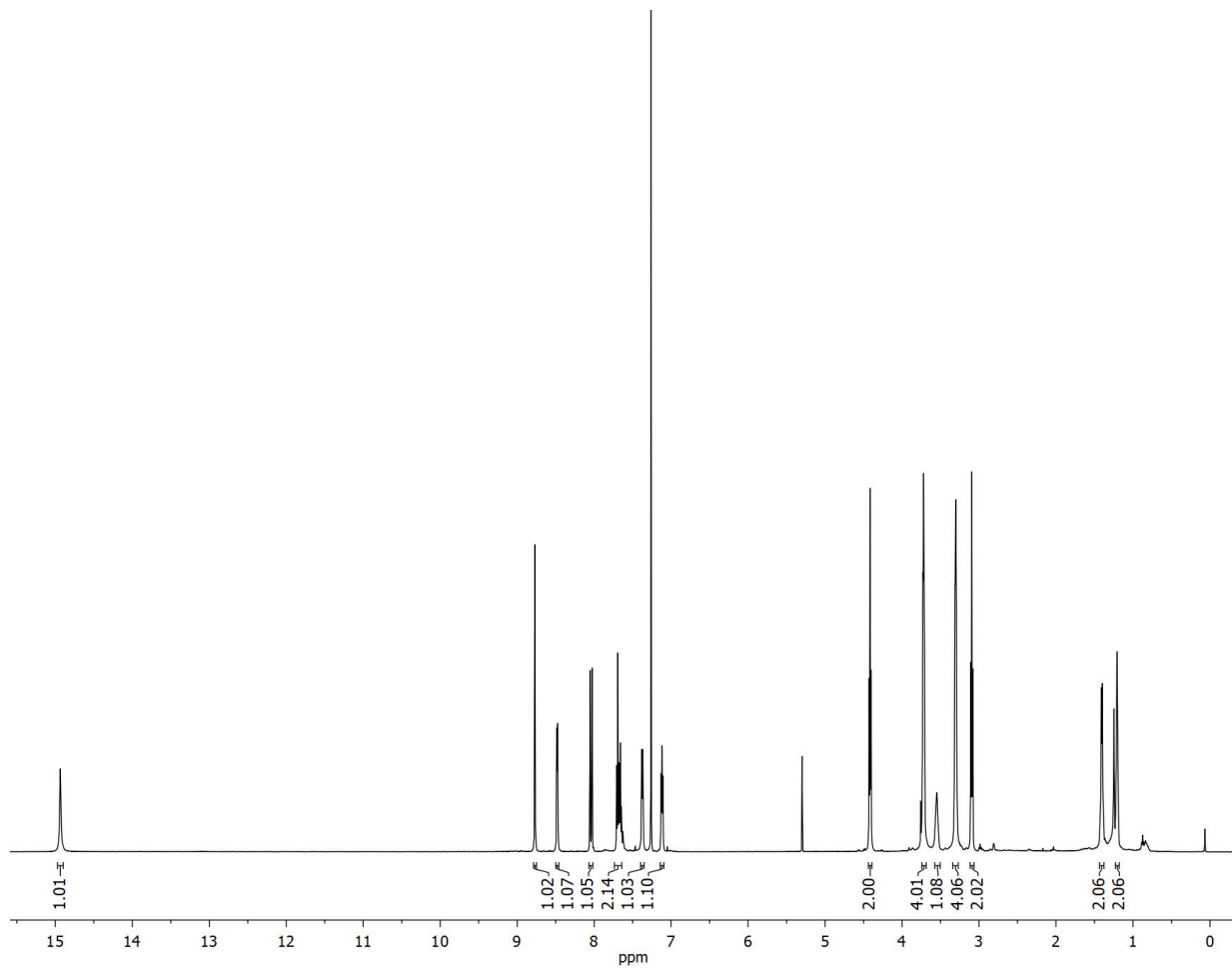


Fig. S42 ¹H NMR (CDCl₃, 500 MHz) of **9**.

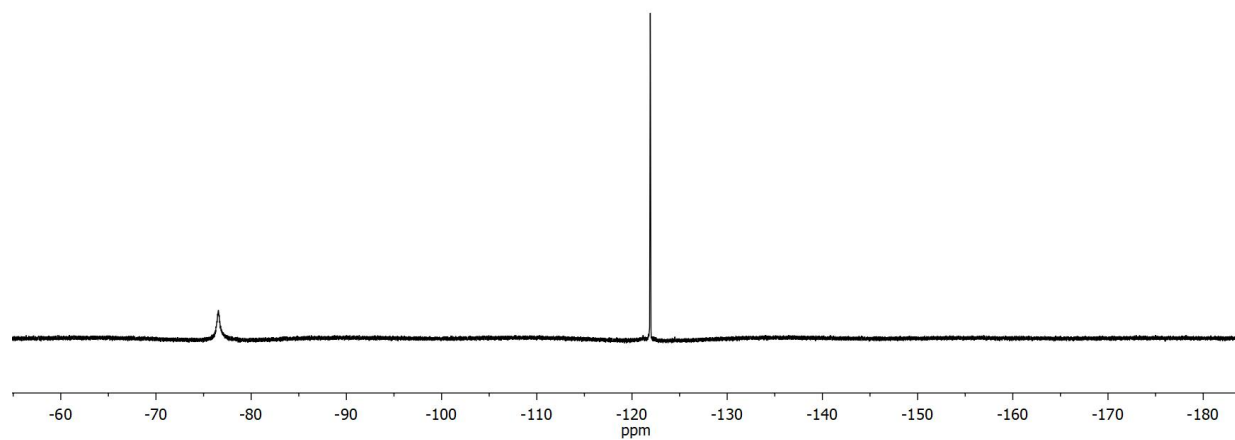


Fig. S43 ^{19}F NMR (CDCl_3 , 470 MHz) of **9**.

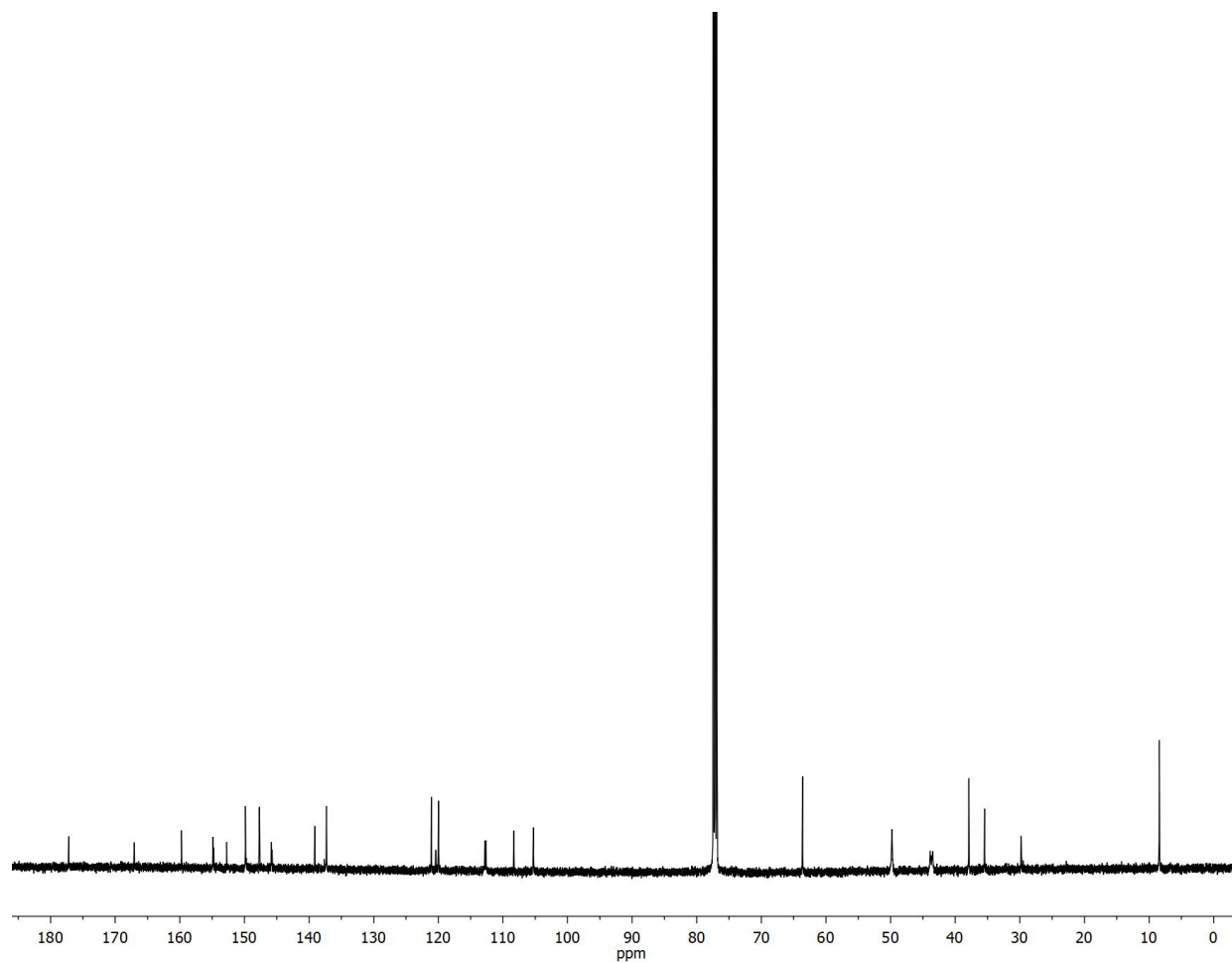


Fig. S44 $^{13}\text{C}\{^1\text{H}\}$ NMR (CDCl_3 , 125 MHz) of **9**.

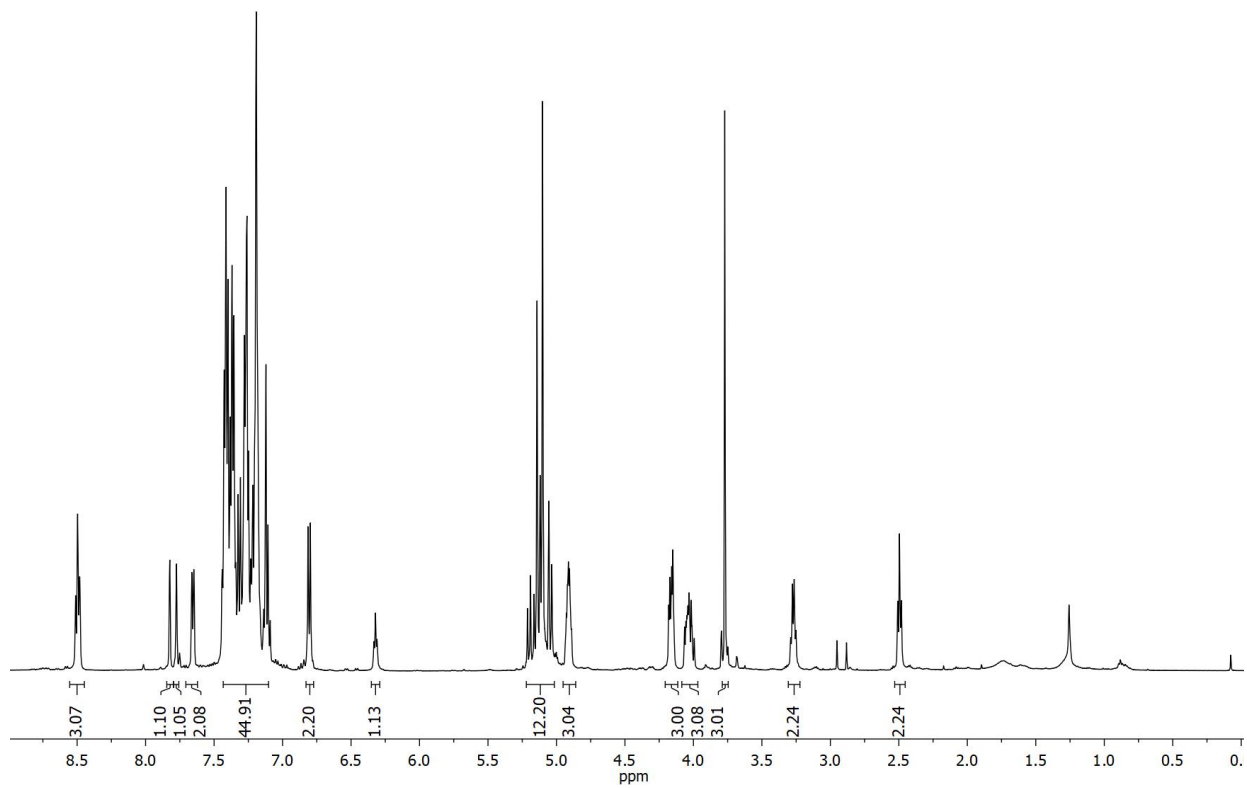


Fig. S45 ¹H NMR (CDCl₃, 500 MHz) of **12**.

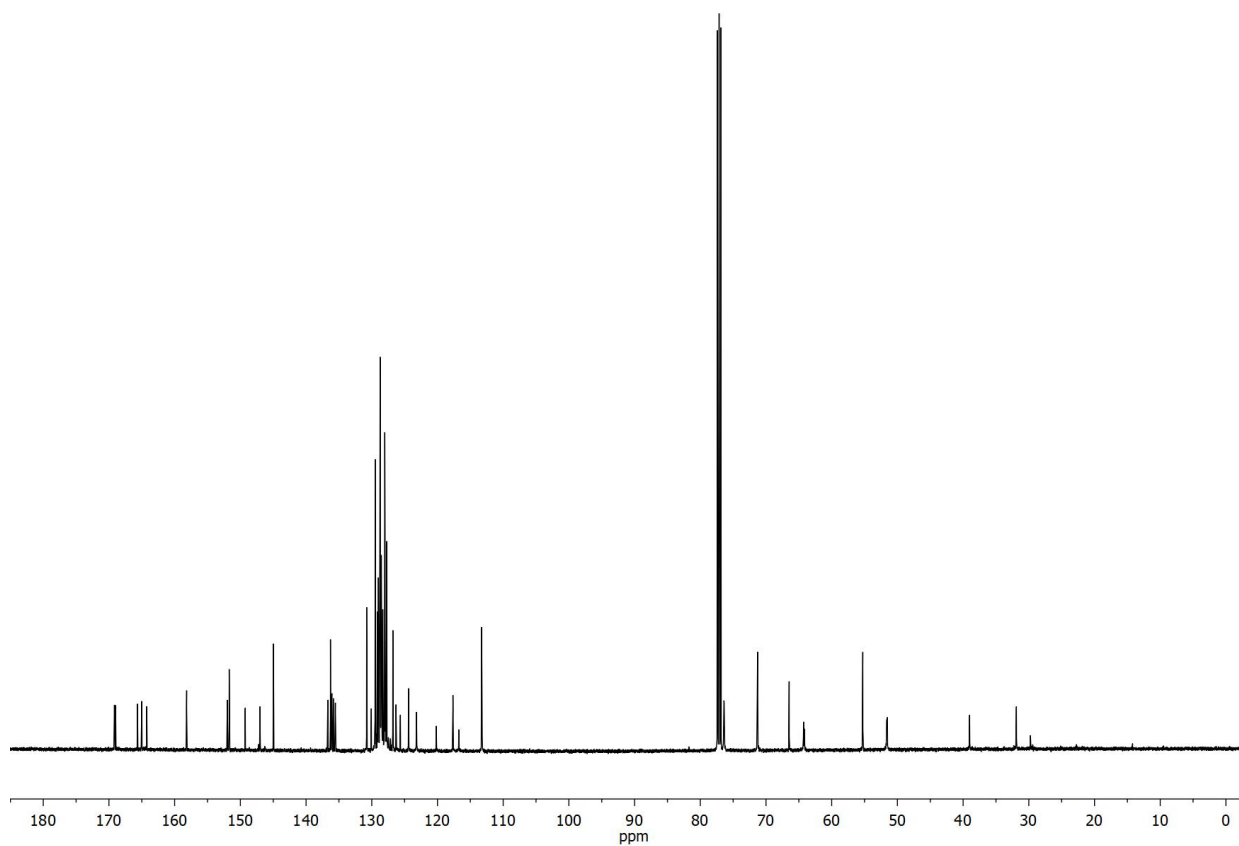


Fig. S46 $^{13}\text{C}\{^1\text{H}\}$ NMR (CDCl_3 , 125 MHz) of **12**.

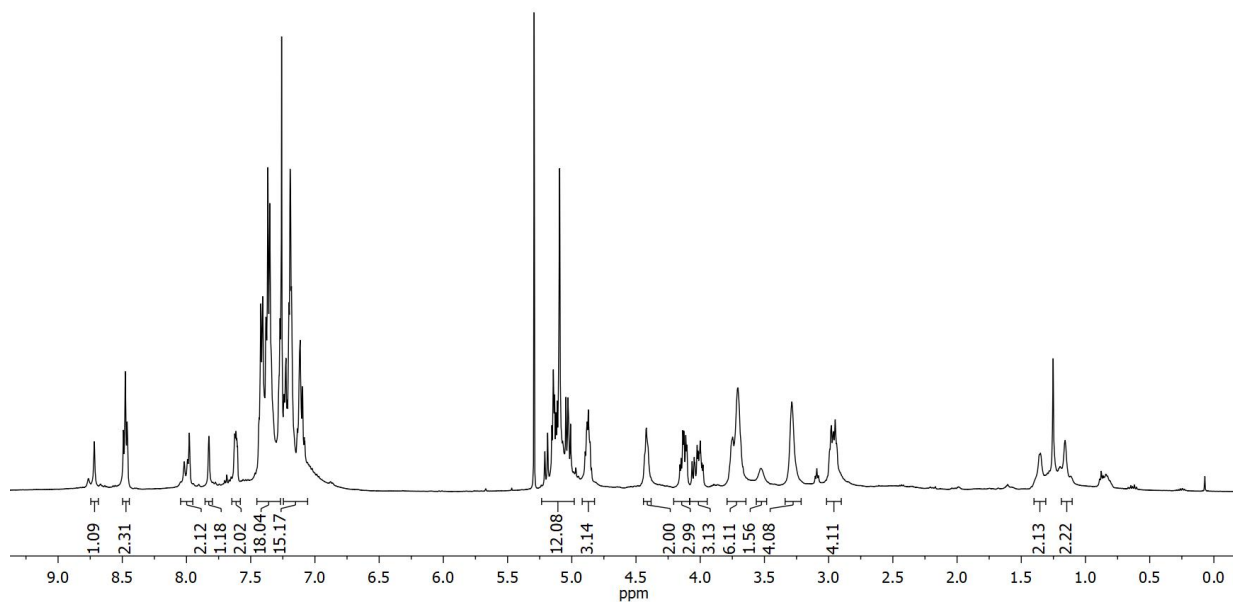


Fig. S47 ¹H NMR (CDCl₃, 500 MHz) of Bn₆Ent-SS-Cipro.

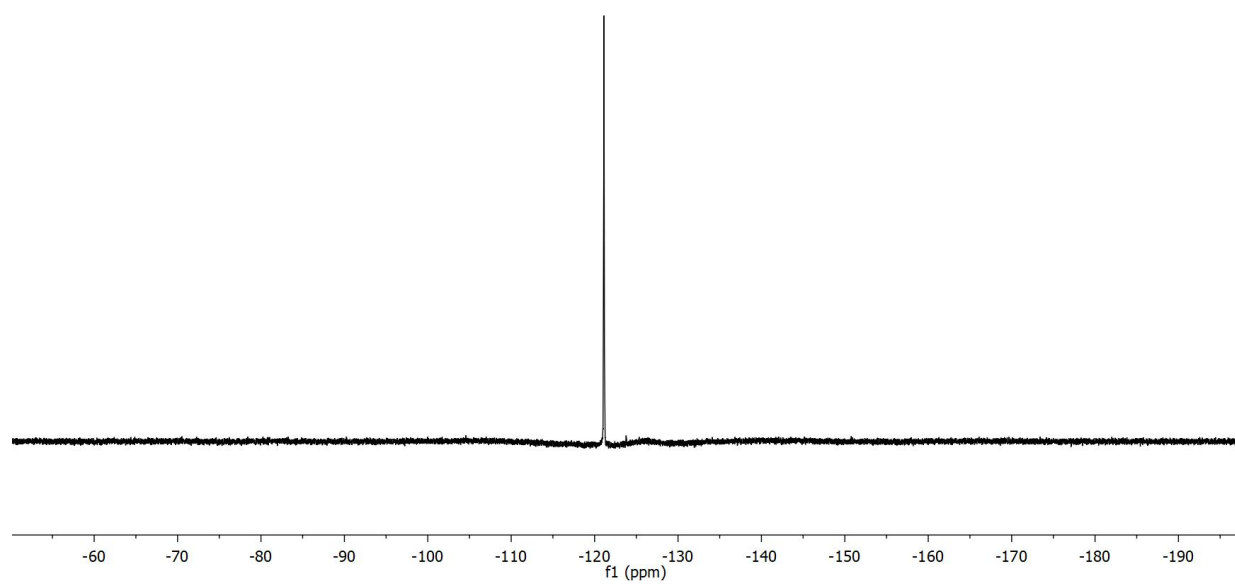


Fig. S48 ^{19}F NMR (CDCl_3 , 470 MHz) of $\text{Bn}_6\text{Ent-SS-Cipro}$.